Universiteit Utrecht

Opleiding Natuur- en Sterrenkunde

Superconductivity with a twist

Bachelor Thesis

Luuk Goode

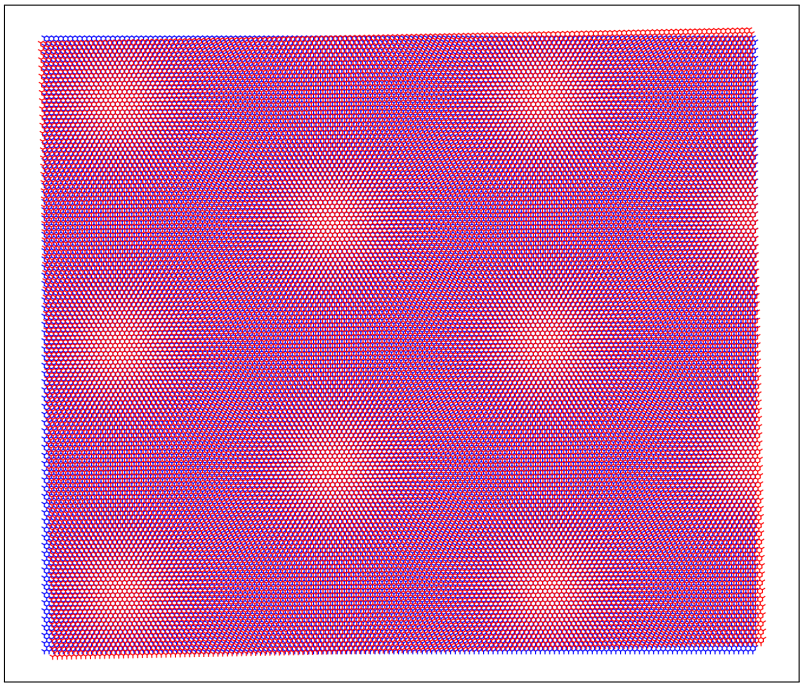

Supervisors:

Prof. Dr. Cristiane de Morais Smith
ITP

MSc. Rodrigo Arouca de Albuquerque
ITP

12-06-2020

Abstract

Superconductivity in high-T_c cuprates is one of the longer lasting mysteries in condensed-matter physics. Cuprates have a complicated chemical structure and display a variety of phenomena in their phase diagram. Because of this, it is not yet fully understood what is the mechanism that is responsible for superconductivity. Recently, superconductivity has been found in twisted bilayer graphene (tBLG), which exhibits a similar phase diagram as high-T_c cuprates, but is purely carbon based. In addition, the doping concentration in tBLG can be varied by means of a gate voltage, which represents a huge advantage in comparison with high-T_c cuprates, for which a new sample must be prepared for each different doping concentration. Therefore, tBLG can possibly serve as a platform to investigate the superconducting mechanism that takes place in high-T_c cuprates. In this thesis, the electronic properties of graphene and bilayer graphene are addressed. Then, a description of superconductivity in relation to its macroscopic properties will be given via the Ginzburg-Landau formalism, and its microscopic properties will be derived using the BCS theory. In the latter approach, the gap equation is derived for general dimensionality and dispersion. The geometry of tBLG will be discussed in relation to its Moiré pattern, after which its dispersion will be examined. Finally, a comparison between tBLG and high-T_c cuprates will be given.

Acknowledgements

First of all, I would like to acknowledge my main supervisor Cristiane, for introducing me to the interesting topic of my thesis and letting me join her research group. I have enjoyed the group meetings, and this is partly thanks to her positivity and kindness towards everyone. My thanks go out to the group members for their comments on my two practise talks, especially to Ozela for giving extra feedback after both of them. In this context, I should also offer my apologies to my friends Noor, Stan, Elise and Ewout, who have been my test subjects during a stage where my talk really was not that good yet... I would like to thank Marino for his clarification on the BCS Hamiltonian, and Lizardo for sharing his thoughts on the gap equation with generic dimensionality and dispersion. I express my gratitude towards my parents, who have supported me during my entire studies, and I thank my roommates, who, due to the Covid outbreak, belonged to the limited few people whom I have seen in person during the period that I wrote this thesis. I also appreciate them for supplying me with coffee, which has been vital during the ending phase of my thesis.

Finally, I would like to thank my daily supervisor Rodrigo, who has been extremely supportive throughout my entire thesis. He is very knowledgeable and was always willing to answer my questions. We have had many interesting discussions, even on weekends, and, at some point, we were chatting until 23:30 on a regular day of the week. Every time we met, Rodrigo was patient and understanding, and at times when I was not feeling so confident about my thesis, I could always continue with a smile after we spoke. Rodrigo has really made the whole research project a fun experience, for which I am very grateful.

Contents

1 Introduction **1**

2 Electronic properties of graphene and bilayer graphene **3**
2.1 Mathematical description of graphene 4
2.2 Reciprocal space 5
2.3 Tight-binding calculation for graphene 6
2.4 Tight-binding calculation for bilayer graphene 9
2.4.1 $\mathbf{A}-\mathbf{A}$ Stacking 9
2.4.2 $\mathbf{A}-\mathbf{B}$ Stacking 10

3 Superconductivity **14**
3.1 Phenomenology of superconductivity 15
3.2 Cooper pairs 17
3.3 Attractive effective electron-electron interaction 18
3.4 Mean-field Hamiltonian 20
3.5 Cooper pair wavefunction 22
3.6 Gap equation 23

4 Twisted bilayer graphene **27**
4.1 Lattice vectors of the Moiré pattern 28
4.2 Hamiltonian of twisted bilayer graphene 31
4.3 Comparison to high-$\mathbf{T_c}$ cuprates 34

5 Conclusion **36**

A Reciprocal space **I**

B Second quantization **II**

C Tight-binding calculation for graphene in first quantization **V**

D Bogoliubov transformation **VII**

1 Introduction

Superconductivity is the physical phenomenon where the electrical resistivity of a material suddenly drops to zero when it is cooled below a certain critical temperature T_c, and the material expels magnetic fields [1–3]. It was first observed in 1911 by the Dutch Nobel prize winner Heike Kamerlingh Onnes in a mercury sample, which had been cooled below 4.2 K [4, 5]. Since then, it has been the quest for physicists to engineer a material with a critical temperature around room temperature.

Superconductivity has many, very useful applications, because it allows for large currents to flow without energy loss or heat production. The dissipationless current opens the possibility to generate increadibly strong magnetic fields, which are for example needed in MRI scanners to increase the imaging resolution [6]. Currently, the strongest MRI scanner tested on a human has a magnetic field of 10.5 T and is located in Minneapolis, USA [7]. However, scans of small animals have been made with a field strength of 21.1 T in Tallahassee, USA [7]. Superconducting electromagnets may find applications in levitated transport too. An operational high speed EDS Maglev train is located in Shanghai, China. This train has clocked a maximal speed of 430 km/h [8], but the record speed of 603 km/h has been reached by another Maglev train during a test run near Mount Fuji [9]. The magnetically levitated trains travel faster, and are also quieter than regular trains because contact between the vehicle and the tracks is eliminated [10]. Another use of superconductivity can be to make energy generators more efficient, reducing their volume and thus their production cost [11]. An example of this is the EU funded EcoSwing project from 2019, where a wind turbine with a superconducting generator was placed in Thyborøn, Denmark [12].

A use of superconductivity can also be found on a more fundamental level, as it is the underlying mechanism for SQUIDs (Superconducting QUantum Interference Devices). A SQUID consists of a superconducting ring with a Josephson junction [13] (a small insulating layer sandwiched between two superconducting elements), and it can measure miniscule magnetic fields of order 10^{-17} T [14]. This can be used in MEG scans that measure brain activity, which is for example done in research on epileptic seizures [15] and Alzheimer's disease [16]. SQUIDs also appear in quantum computers, because a series of SQUIDs allows for an entangled quantum state [17]. Quantum computers [18] are expected to be able to perform complicated calculations that are not possible on regular computers, such as biomolecular modeling [19] and effective database searching [20].

If a material would exist that displays superconductivity at room temperature, these applications would have much lower production costs than they have now, since the need for extensive cooling mechanisms would be eliminated. Moreover, it would become thinkable to incorporate superconducting materials in everyday electronics, making them faster and less energy-consuming. As of today however, the highest critical temperature that has been whitnessed in a superconductor at atmospheric pressure is about 133 K [21]. This is the critical temperature for high-T_c cuprates in the $\mathrm{Hg-Ba-Ca-Cu-O}$ system. These materials have a complicated chemical structure, and despite the abundance of work done in the field (over 10.000 results pop up when searching on the topic "cuprate" in Ref. [22], and

the original paper from 1986 about the discovery of high-T_c cuprates has been cited over 17500 times [23]), it is currently still unclear what mechanism is responsible for the superconductivity [24]. It is equally unclear how the different effects that take place in the system are related to superconductivity [25]. Experimental research on high-T_c cuprates also faces a difficulty, because investigating their phase diagrams requires doping, which changes their chemical properties [26]. To gain more insight in high-T_c superconductivity, it is desirable to investigate materials that have a phase diagram similar to that of high-T_c cuprates, but that are less complicated and do not require chemical doping. It has recently been found that the two-dimensional material twisted bilayer graphene meets these requirements [27,28].

Twisted bilayer graphene (tBLG) consists of two layers of graphene stacked upon each other with a relative twist [27,28]. If a twist of 1.1 degrees is introduced between the layers, superconductivity can take place at relatively high temperatures compared to the charge carrier density. This was first reported by Cao et al. in 2018 [27]. Because graphene can be easily isolated from graphite, reasearch on graphene-based materials such as tBLG is very accessible. This possibly provides a platform to understand the superconductivity mechanism in high-T_c cuprates. Twisted bilayer graphene is a hot topic in physics (with over 600 hits when searching for the topic "twisted bilayer graphene" in Ref. [22] since the first paper about the electronic properties of tBLG in 2007 [29]), and it is still an open problem in physics to find out how the superconductivity in this material arises. Hopefully, new insights on superconductivity in tBLG will bring us one step closer towards achieving room-temperature superconductors.

In this thesis, the electronic properties of graphene and its bilayer variant will be presented in Chapter 2. In Chapter 3, we will discuss some properties of superconductivity and investigate how to treat interactions in a system using BCS theory. Then, we will discuss the electronic properties of tBLG in Chapter 4 and make a comparison between its phase diagram and that of high-T_c cuprates. The thesis will be concluded in Chapter 5.

2 Electronic properties of graphene and bilayer graphene

Graphene is a 2D material made of carbon atoms that are arranged into a honeycomb lattice. It has many interesting properties: It is extremely strong (breaking strength 42 Nm^{-2}) and stiff (Young's modulus 1.0 TPa) [30], whilst maintaining its elasticity, making it impermeable to gases [31]. It is also transparent (opacity $2.3 \pm 0.1\%$) [32], and has both high electrical conductivity at room temperature (charge carrier mobility $\approx 2{*}10^5$ $\mathrm{cm}^2(\mathrm{Vs})^{-1}$) [33] and high thermal conductivity (exceeding 2000 $\mathrm{W(mK)}^{-1}$) [34]. In addition to this, graphene is very thin and light, and there exist methods for cheap, environment-friendly production [35, 36].

Because of its useful properties, graphene is expected to have various applications in different fields. For example, in nanoelectronics, graphene can be used in the production of nanoscale transistors [37]. It could also be used in the production of transparent, flexible and relatively cheap solar cells [38], and it may find biomedical applications in drug delivery, tumor therapy and personalized medicines [39]. Furthermore, it may be used in future touch screens [40] and it could be added in various composites [41]. These examples are only a few of the many applications of graphene.

Until 2004, two-dimensional materials were thought to exist only in theory due to the Mermin-Wagner theorem [42]. However, in 2004, Novoselov and Geim had succesfully isolated graphene from its stacked 3D variant graphite using mechanical exfoliation [43] (ripples in graphene explain why it can maintain its crystal structure [44]). The discovery of stable graphene was revolutionary because it opened the possibility to easily perform research on 2D materials. Since 2004, all kinds of 2D crystals have been prepared using mechanical cleavage [45], and nowadays, the synthesis of 2D materials includes both top-down (when they are retrieved from the 3D bulk) and bottom-up (when they are constructed from smaller components) methods [46, 47].

Two-dimensional materials enable the use of scanning probing techniques, which can give a complete characterization of the properties of the material (since it is only one atom thick) and can also be used to investigate local properties [48, 49]. Typically, these properties are very different from 3D materials [48]. Since graphene usually lies on a substrate, the properties of the latter (such as the dielectric constant) also influence the electron transport in graphene [50]. Furthermore, the electronic properties of 2D materials can change drastically when they are combined with a second sheet of material [51]. With this, heterostructures can be created of which we can engineer the properties [52]. This gave rise to the idea of combining two layers of graphene to form bilayer graphene, and it has been found that the twist angle between the sheets vastly modifies its electronic properties.

In this chapter, we will focus on the electronic properties of graphene and its bilayer variant. A mathematical description of the graphene lattice will be given in Section 2.1, followed by a description of its First Brillouin zone in Section 2.2. Then, a tight-binding calculation will be done using second quantization in Section 2.3, to obtain the dispersion relation of monolayer graphene. In Section 2.4, the dispersion relations of two types of bilayer graphene will be presented.

2.1 Mathematical description of graphene

Graphene's honeycomb lattice can be described as a triangular Bravais lattice with a two-particle unit cell and spacing a. Thus, the honeycomb lattice is composed of two triangular sublattices, denoted by A and B. Nearest neighbors in the honeycomb lattice are separated by a distance $d = a/\sqrt{3}$ (see Fig. 1).

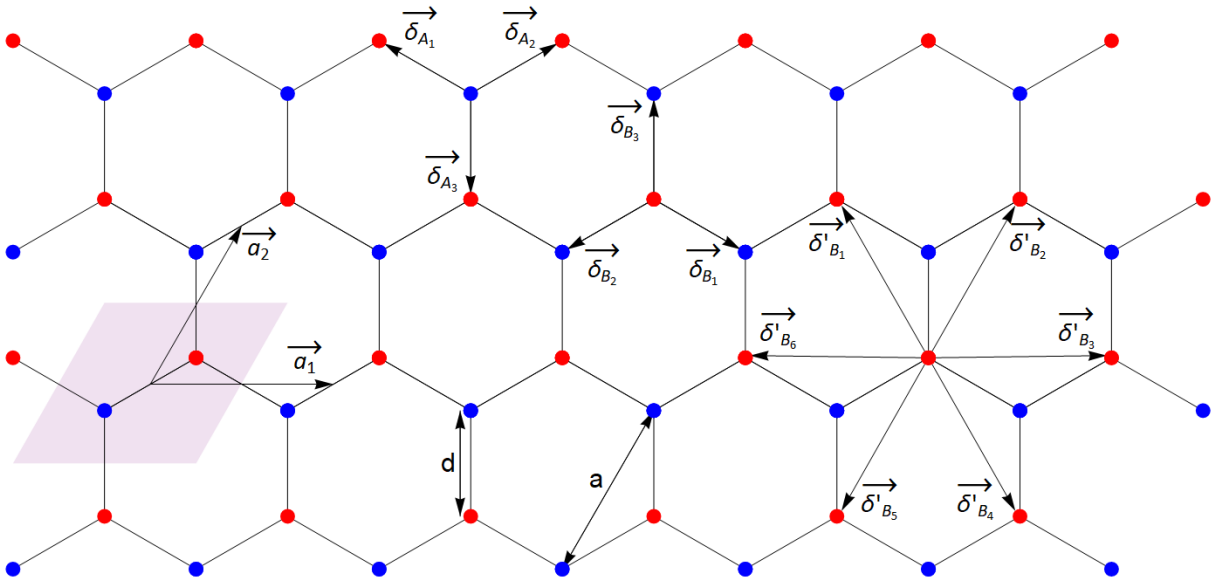

Figure 1: Direct lattice of graphene. The unit cell is indicated by the light-purple diamond on the left of the figure, with primitive lattice vectors $\vec{a_1}$ and $\vec{a}_2$. The blue dots correspond to the triangular sublattice A and the red ones to B. The lattice spacing of the triangular lattices are given by a and the distance between nearest neighbors in the honeycomb lattice is given by d. The $\vec{\delta}$ represent nearest-neighbor vectors whereas the $\vec{\delta}'$ represent next-nearest-neighbor vectors.

The primitive lattice vectors of the graphene lattice are then given by:

$$\begin{aligned} \vec{a}_1 &= a \begin{pmatrix} 1 \\ 0 \end{pmatrix}, \\ \vec{a}_2 &= \frac{a}{2} \begin{pmatrix} 1 \\ \sqrt{3} \end{pmatrix}. \end{aligned} \tag{1}$$

This leads to the nearest-neighbor vectors

$$\begin{aligned} \vec{\delta}_{A_1} &= -\vec{\delta}_{B_1} = \frac{1}{3}\vec{a}_2 - \frac{2}{3}\vec{a}_1, \\ \vec{\delta}_{A_2} &= -\vec{\delta}_{B_2} = \frac{1}{3}\vec{a}_1 + \frac{1}{3}\vec{a}_2, \\ \vec{\delta}_{A_3} &= -\vec{\delta}_{B_3} = \frac{1}{3}\vec{a}_1 - \frac{2}{3}\vec{a}_2, \end{aligned} \tag{2}$$

and the next-nearest-neighbor vectors

$$\begin{aligned}\vec{\delta}'_{A_1} = -\vec{\delta}'_{A_4} = \vec{\delta}'_{B_1} = -\vec{\delta}'_{B_4} = \vec{a}_2 - \vec{a}_1,\\ \vec{\delta}'_{A_2} = -\vec{\delta}'_{A_5} = \vec{\delta}'_{B_2} = -\vec{\delta}'_{B_5} = \vec{a}_2,\\ \vec{\delta}'_{A_3} = -\vec{\delta}'_{A_6} = \vec{\delta}'_{B_3} = -\vec{\delta}'_{B_6} = \vec{a}_1.\end{aligned} \tag{3}$$

2.2 Reciprocal space

The reciprocal space (more explanations about this can be found in appendix A) of graphene is again a honeycomb lattice, of which the primitive lattice vectors are given by

$$\begin{aligned}\vec{b}_1 &= \frac{2\pi}{\sqrt{3}a}\begin{pmatrix}\sqrt{3}\\ -1\end{pmatrix},\\ \vec{b}_2 &= \frac{4\pi}{\sqrt{3}a}\begin{pmatrix}0\\ 1\end{pmatrix}.\end{aligned} \tag{4}$$

This leads to the six corners of the First Brillouin zone (see Fig. 2) having coordinates $(\pm\frac{4\pi}{3a}, 0), (\pm\frac{2\pi}{3a}, \pm\frac{2\pi}{\sqrt{3}a})$. The corners $(\frac{4\pi}{3a}, 0), (-\frac{2\pi}{3a}, \frac{2\pi}{\sqrt{3}a}), (-\frac{2\pi}{3a}, -\frac{2\pi}{\sqrt{3}a})$ are related by each other via reciprocal lattice vectors and are therefore all given the label K. Similarly, the K' points are given by $(-\frac{4\pi}{3a}, 0), (\frac{2\pi}{3a}, \frac{2\pi}{\sqrt{3}a}), (\frac{2\pi}{3a}, -\frac{2\pi}{\sqrt{3}a})$.

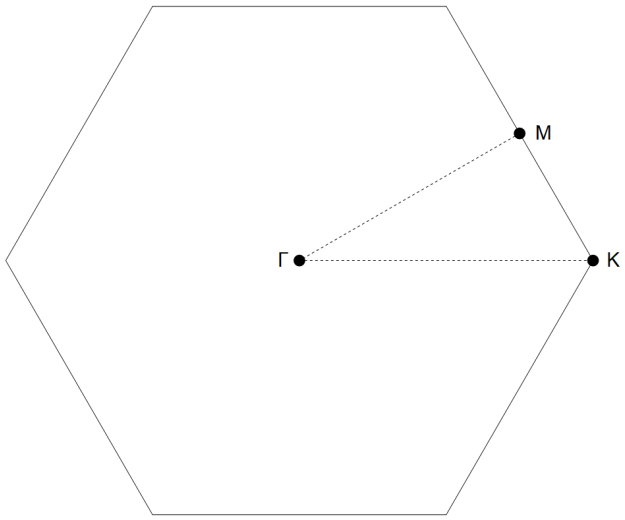

Figure 2: First Brillouin zone of graphene, with the Γ point at $(0, 0)$, the K point at $(\frac{4\pi}{3a}, 0)$ and the M point at $(\frac{\pi}{a}, \frac{\pi}{\sqrt{3}a})$.

In the First Brillouin zone, three points are of special interest. These are the Γ point (located in the middle of the First Brillouin zone), the K point (on one of the corners), and the M point (on the middle of one of the edges). These points are of high symmetry, so it is expected that any interesting behavior of the system should occur in the neighborhood of one of these

points. Therefore, dispersion relations are plotted along the path connecting them. Let $s \in [0,3]$, then a parametrization for the path $\Gamma - K - M - \Gamma$ is given by

$$\begin{pmatrix} k_x \\ k_y \end{pmatrix} = \begin{cases} s \begin{pmatrix} \frac{4\pi}{3a} \\ 0 \end{pmatrix} & \text{for } s \in [0,1), \\ \begin{pmatrix} \frac{4\pi}{3a} \\ 0 \end{pmatrix} + (s-1) \begin{pmatrix} -\frac{\pi}{3a} \\ \frac{\pi}{\sqrt{3}a} \end{pmatrix} & \text{for } s \in [1,2), \\ \begin{pmatrix} \frac{\pi}{a} \\ \frac{\pi}{\sqrt{3}a} \end{pmatrix} - (s-2) \begin{pmatrix} \frac{\pi}{a} \\ \frac{\pi}{\sqrt{3}a} \end{pmatrix} & \text{for } s \in [2,3]. \end{cases} \tag{5}$$

2.3 Tight-binding calculation for graphene

In second quantization, all operators can be written in terms of creation and annihilation operators $c^\dagger$ and c (see appendix B). For fermions, their eigenvalues are given by

$$\begin{aligned} c^\dagger |0\rangle &= |1\rangle, \qquad & c|0\rangle &= 0, \\ c^\dagger |1\rangle &= 0, \qquad & c|1\rangle &= |0\rangle. \end{aligned} \tag{6}$$

For the graphene lattice, we will characterize the electrons using the sets of quantum numbers $L, \vec{R}_l$ and Σ. The quantum number $l \in L$ can be equal to either A or B, which indicates in which sublattice the electron lives. The quantum number $\vec{r} \in \vec{R}_l$ denotes the site at which the electron is sitting in sublattice l, and $\sigma \in \Sigma$ has either value $1/2$ or $-1/2$, which denotes the spin (which is a conserved quantity).

In the tight-binding approximation, we can write our Hamiltonian as

$$\mathcal{H} = \sum_{l,l',\langle\langle \vec{r},\vec{r}' \rangle\rangle,\sigma} c^\dagger_{l,\vec{r},\sigma} c_{l',\vec{r}',\sigma} \langle l,\vec{r},\sigma|\mathcal{H}|l',\vec{r}',\sigma\rangle, \tag{7}$$

where $\langle\langle \vec{r},\vec{r}' \rangle\rangle$ indicates that the sum is restricted to $\vec{r}$ and $\vec{r}'$ being next-nearest neighbors at the most. Now, assume that

$$\langle l,\vec{r},\sigma|\mathcal{H}|l',\vec{r}',\sigma\rangle = \begin{cases} \epsilon_0 & \text{when } \vec{r} = \vec{r}', \\ t & \text{when } \vec{r} \text{ and } \vec{r}' \text{ represent nearest neighbors,} \\ t' & \text{when } \vec{r} \text{ and } \vec{r}' \text{ represent next-nearest neighbors,} \\ 0 & \text{else.} \end{cases} \tag{8}$$

Then, we can write our Hamiltonian as

$$\begin{aligned} \mathcal{H} &= \epsilon_0 \sum_{l,\vec{r},\sigma} c^\dagger_{l,\vec{r},\sigma} c_{l,\vec{r},\sigma} + t \sum_{\substack{l \neq l' \\ \vec{r},j,\sigma}} c^\dagger_{l,\vec{r},\sigma} c_{l',\vec{r}+\vec{\delta}_{l_j},\sigma} + t' \sum_{l,\vec{r},j,\sigma} c^\dagger_{l,\vec{r},\sigma} c_{l,\vec{r}+\vec{\delta}'_{l_j},\sigma} = \\ &= \mathcal{H}_0 + \mathcal{H}_{nn} + \mathcal{H}_{nnn}, \end{aligned} \tag{9}$$

with $\vec{\delta}, \vec{\delta}'$ defined in Section 2.1. It will be easier to diagonalise the Hamiltonian when it is written as a function of $\vec{k}$, so we will apply a Fourier transformation to find

$$\mathcal{H}_0 = \epsilon_0 \sum_{l,\sigma} \sum_{\vec{k}} c^\dagger_{l,\vec{k},\sigma} c_{l,\vec{k},\sigma}, \tag{10}$$

$$\mathcal{H}_{nn} = t \sum_{l \neq l',\sigma} \sum_{\vec{k}} c^{\dagger}_{l,\vec{k},\sigma} c_{l',\vec{k},\sigma} \sum_j e^{i\vec{\delta}_{l_j}\cdot\vec{k}}, \tag{11}$$

$$\mathcal{H}_{nnn} = t' \sum_{l,\sigma} \sum_{\vec{k}} c^{\dagger}_{l,\vec{k},\sigma} c_{l,\vec{k},\sigma} \sum_j e^{i\vec{\delta}'_{l_j}\cdot\vec{k}}. \tag{12}$$

Writing this in matrix form (such that $\langle \vec{r}_l, \sigma | \mathcal{H} | \vec{r}\,'_{l'}, \sigma \rangle = H_{ll'}$) yields

$$H = \begin{array}{c} \\ A \\ B \end{array} \begin{array}{c} \begin{array}{cc} A & B \end{array} \\ \begin{pmatrix} \epsilon_0 + t' \sum_j e^{i\vec{\delta}'_{A_j}\cdot\vec{k}} & t \sum_j e^{i\vec{\delta}_{A_j}\cdot\vec{k}} \\ t \sum_j e^{i\vec{\delta}_{B_j}\cdot\vec{k}} & \epsilon_0 + t' \sum_j e^{i\vec{\delta}'_{B_j}\cdot\vec{k}} \end{pmatrix} \end{array} = \tag{13}$$

$$= d_{\mathbb{1}}(\vec{k})\mathbb{1} + d_x(\vec{k})\tau_x + d_y(\vec{k})\tau_y,$$

where

$$\begin{aligned} d_{\mathbb{1}}(\vec{k}) &= \epsilon_0 + t' \sum_j e^{i\vec{\delta}'_{A_j}\cdot\vec{k}}, \\ d_x(\vec{k}) &= t \sum_j \cos(\delta_{A_j}), \\ d_y(\vec{k}) &= -t \sum_j \sin(\delta_{A_j}), \end{aligned} \tag{14}$$

and τ_x, τ_y are Pauli matrices. When we write

$$\begin{aligned} \gamma(\vec{k}) &= \sqrt{\sum_j e^{i\vec{\delta}_{A_j}\cdot\vec{k}} \sum_j e^{i\vec{\delta}_{B_j}\cdot\vec{k}}} = \\ &= \sqrt{3 + 2\cos(\vec{k}\cdot\vec{a}_1) + 2\cos(\vec{k}\cdot\vec{a}_2) + 2\cos(\vec{k}\cdot(\vec{a}_1 - \vec{a}_2))}, \\ \gamma'(\vec{k}) &= \sum_j e^{i\vec{\delta}'_{A_j}\cdot\vec{k}} = \sum_j e^{i\vec{\delta}'_{B_j}\cdot\vec{k}} = \\ &= 2\left[\cos(\vec{k}\cdot\vec{a}_1) + \cos(\vec{k}\cdot\vec{a}_2) + \cos\left(\vec{k}\cdot(\vec{a}_1 - \vec{a}_2)\right)\right], \end{aligned} \tag{15}$$

and diagonalize the matrix from Eq. (13), we are led to the eigenvalues

$$E(\vec{k}) = \epsilon_0 + t'\gamma'(\vec{k}) \pm t\gamma(\vec{k}). \tag{16}$$

The dispersion relation is plotted in Fig. 3. The function $\gamma^2(\vec{k})$ can be expanded around the K-point, which leads to $\gamma^2(\vec{K} + \delta\vec{k}) \approx 3a^2t^2|\delta\vec{k}|^2/4$. Then, γ is linear up to first order in $\vec{k}$, as well as γ'. Hence, the dispersion relation is linear in the vicinity of a K-point, as can be recognized in Fig. 3 by the Dirac cones. This can also be seen by expanding the matrix from Eq. (13) around $\vec{K}$ and putting it in standard Dirac form via a canonical transformation [3], such that

$$H_{Dirac} = (\epsilon_0 - 3t')\mathbb{1} + \frac{1}{2}\sqrt{3}at\left[(\delta k_x)\tau_x + (\delta k_y)\tau_y\right]. \tag{17}$$

If we diagonalise H_{Dirac}, we retrieve the eigenvalues $E = (\epsilon_0 - 3t') \pm \hbar v_F|\delta\vec{k}|$ with $v_F = \sqrt{3}at/(2\hbar)$ the Fermi velocity. This linearity implies that the electrons near the K-point behave like massless particles with speed v_F.

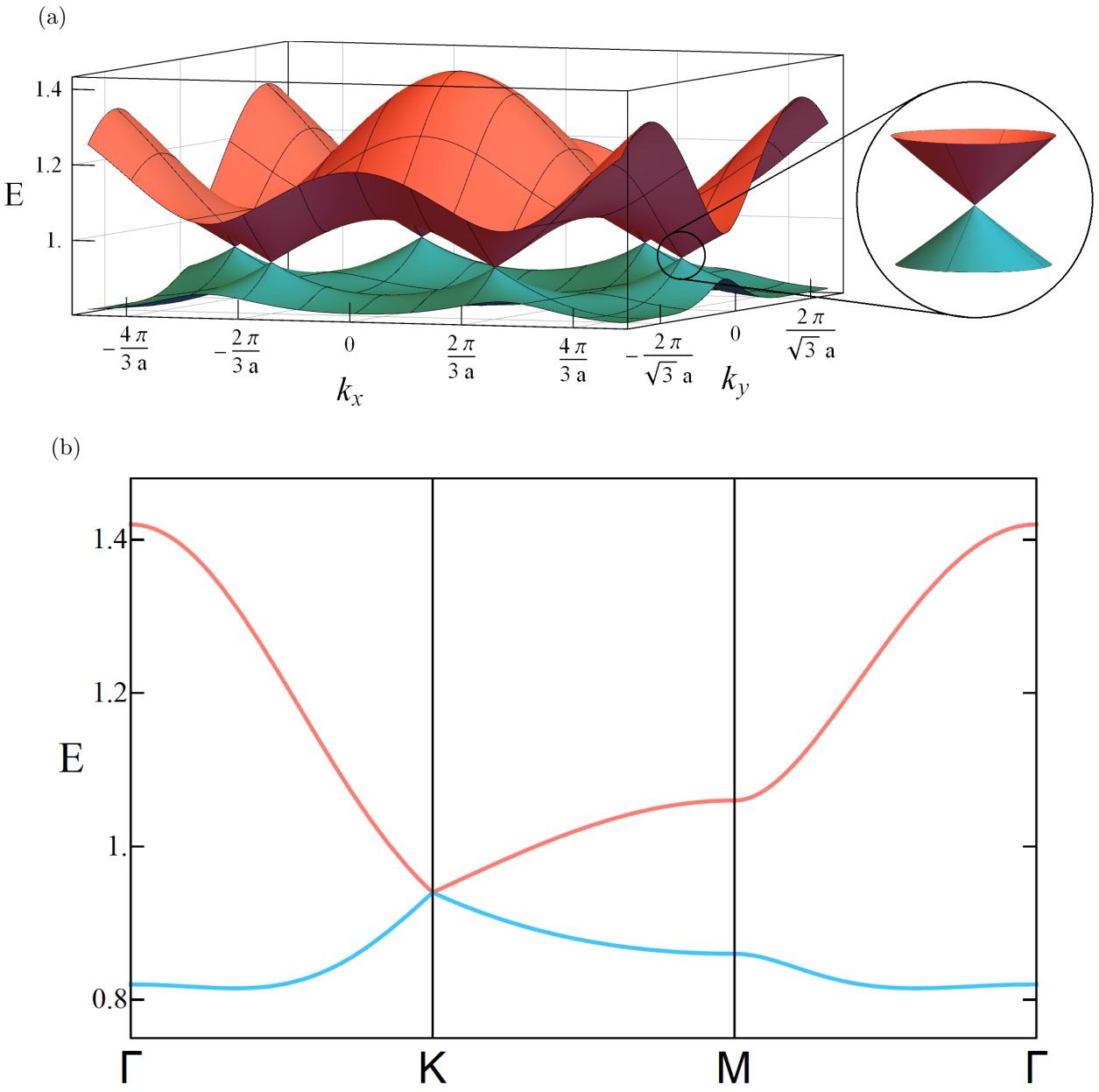

Figure 3: (a) Dispersion relation of monolayer graphene with next-nearest-neighbor hopping. The inset shows the linear dispersion around one of the K points. (b) Dispersion relation as going through the First Brillouin zone by following the path $\Gamma - K - M - \Gamma$. For these panels, the parameter values $\epsilon_0 = 1, t = 0.1$ and $t' = 0.02$ were used.

2.4 Tight-binding calculation for bilayer graphene

When stacking two layers of graphene on top of each other, two typical orderings can occur. The layers can either be directly on top of each other without any translation in the $x-y$ plane, or there can be a shift between the layers, such that some atoms have no vertical neighbor and instead lay above the center of a honeycomb cell from the other layer. The first type of stacking is called an $A-A$ stacking, and the second type an $A-B$ stacking (see Fig. 4).

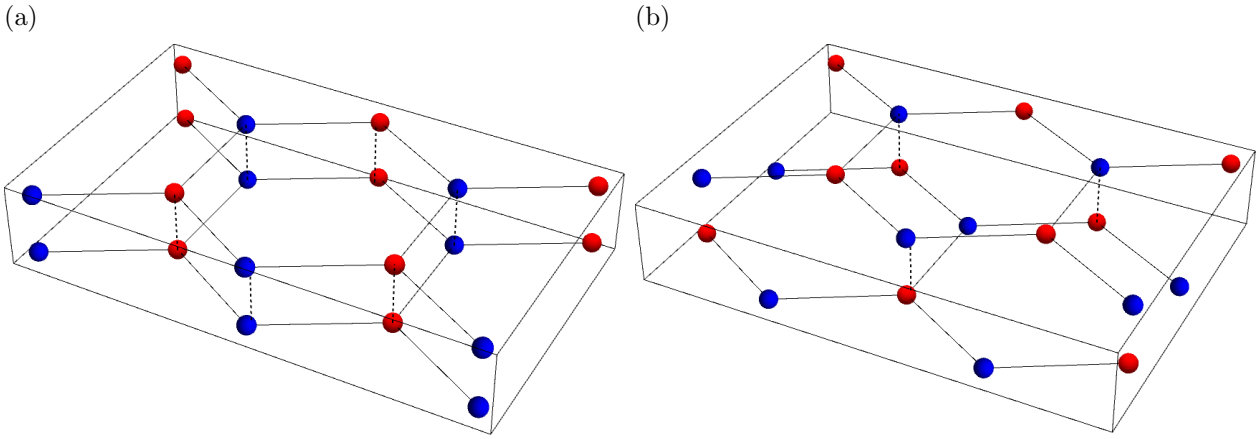

Figure 4: Stacking of bilayer graphene. The blue sites are part of the sublattice A, and the red sites of sublattice B. (a) $A-A$ stacking. (b) $A-B$ stacking.

To extend the tight-binding calculation to bilayer graphene, we introduce another set of quantum numbers M such that $m \in M$ has either value 1 or 2, which distinguishes the two layers. The set $\vec{R}_l^m$ describing the sites now also depends on the layer. This changes our assumptions about the Hamiltonian to

$$\langle m,l,\vec{r},\sigma|\mathcal{H}|m',l',\vec{r}',\sigma\rangle = \begin{cases} \epsilon_0 & \text{when } m=m' \text{ and } \vec{r}=\vec{r}', \\ t & \text{when } m=m' \text{ and } \vec{r},\vec{r}' \text{ represent nearest neighbors}, \\ t' & \text{when } m=m' \text{ and } \vec{r},\vec{r}' \text{ represent next-nearest neighbors}, \\ t_\perp & \text{when } m\neq m' \text{ and } \vec{r}=\vec{r}', \\ 0 & \text{else.} \end{cases} \tag{18}$$

2.4.1 A – A Stacking

We assume an $A-A$ stacking and introduce the partial Hamiltonian $\mathcal{H}_\perp$ that describes the inter-layer hopping:

$$\mathcal{H}_\perp = t_\perp \sum_{\substack{m\neq m' \\ l,\vec{r},\sigma}} c^\dagger_{m,l,\vec{r},\sigma} c_{m',l,\vec{r},\sigma} = t_\perp \sum_{\substack{m\neq m' \\ l,\sigma}} \sum_{\vec{k}} c^\dagger_{m,l,\vec{k},\sigma} c_{m',l,\vec{k},\sigma}. \tag{19}$$

Adding this to the Hamiltonian yields

$$H_{AA} = \begin{array}{c} \\ A^1 \\ B^1 \\ A^2 \\ B^2 \end{array} \begin{array}{c} \begin{array}{cccc} A^1 & B^1 & A^2 & B^2 \end{array} \\ \begin{pmatrix} \epsilon_0 + t'\gamma'(\vec{k}) & t\sum_i e^{\vec{\delta}_{A_i}\cdot\vec{k}} & t_\perp & 0 \\ t\sum_i e^{\vec{\delta}_{B_i}\cdot\vec{k}} & \epsilon_0 + t'\gamma'(\vec{k}) & 0 & t_\perp \\ t_\perp & 0 & \epsilon_0 + t'\gamma'(\vec{k}) & t\sum_i e^{\vec{\delta}_{A_i}\cdot\vec{k}} \\ 0 & t_\perp & t\sum_i e^{\vec{\delta}_{B_i}\cdot\vec{k}} & \epsilon_0 + t'\gamma'(\vec{k}) \end{pmatrix} \end{array} =$$

$$= t_\perp\big(\tau_x \otimes \mathbb{1}\big) + \mathbb{1} \otimes \big(d_{\mathbb{1}}(\vec{k})\mathbb{1} + d_x(\vec{k})\tau_x + d_y(\vec{k})\tau_y\big).$$

Note that for $t_\perp = 0$, the matrix splits into two blocks, so if there is no hopping between the layers, they decouple and lead to a twofold degenerate case of the monolayer dispersion relation. The matrix leads to the eigenvalues

$$E(\vec{k}) = \epsilon_0 + t'\gamma'(\vec{k}) \pm \sqrt{t_\perp^2 + t^2\gamma^2(\vec{k}) \pm 2\sqrt{t_\perp^2 t^2\gamma^2(\vec{k})}}. \tag{20}$$

The dispersion relation is plotted in Fig. 5.

2.4.2 A – B Stacking

We could also have assumed an $A - B$ stacking. In this way, vertical hopping can only take place between A type sites of the first layer and B type sites of the second layer. This leads to

$$\mathcal{H}_\perp = t_\perp \sum_{\substack{m\neq m' \\ l\neq l',\vec{r},\sigma}} c^\dagger_{m,l,\vec{r},\sigma} c_{m',l',\vec{r},\sigma} = t_\perp \sum_{\substack{m\neq m' \\ l\neq l',\sigma}} \sum_{\vec{k}} c^\dagger_{l,m,\vec{k},\sigma} c_{l',m',\vec{k},\sigma}. \tag{21}$$

In matrix representation, the complete Hamiltonian then reads

$$H_{AB} = \begin{array}{c} \\ A^1 \\ B^1 \\ A^2 \\ B^2 \end{array} \begin{array}{c} \begin{array}{cccc} A^1 & B^1 & A^2 & B^2 \end{array} \\ \begin{pmatrix} \epsilon_0 + t'\gamma'(\vec{k}) & t\sum_i e^{\vec{\delta}_{A_i}\cdot\vec{k}} & 0 & 0 \\ t\sum_i e^{\vec{\delta}_{B_i}\cdot\vec{k}} & \epsilon_0 + t'\gamma'(\vec{k}) & t_\perp & 0 \\ 0 & t_\perp & \epsilon_0 + t'\gamma'(\vec{k}) & t\sum_i e^{\vec{\delta}_{A_i}\cdot\vec{k}} \\ 0 & 0 & t\sum_i e^{\vec{\delta}_{B_i}\cdot\vec{k}} & \epsilon_0 + t'\gamma'(\vec{k}) \end{pmatrix} \end{array} =$$

$$= \frac{t_\perp}{2}\big(\tau_x \otimes \tau_x + \tau_y \otimes \tau_y\big) + \mathbb{1} \otimes \big(d_{\mathbb{1}}(\vec{k})\mathbb{1} + d_x(\vec{k})\tau_x + d_y(\vec{k})\tau_y\big),$$

and the eigenvalues (plotted in Fig. 6) are

$$E(\vec{k}) = \epsilon_0 + t'\gamma'(\vec{k}) \pm \sqrt{\frac{1}{2}t_\perp^2 + t^2\gamma^2(\vec{k}) \pm \sqrt{t_\perp^2 t^2\gamma^2(\vec{k}) + \frac{1}{4}t_\perp^2}}. \tag{22}$$

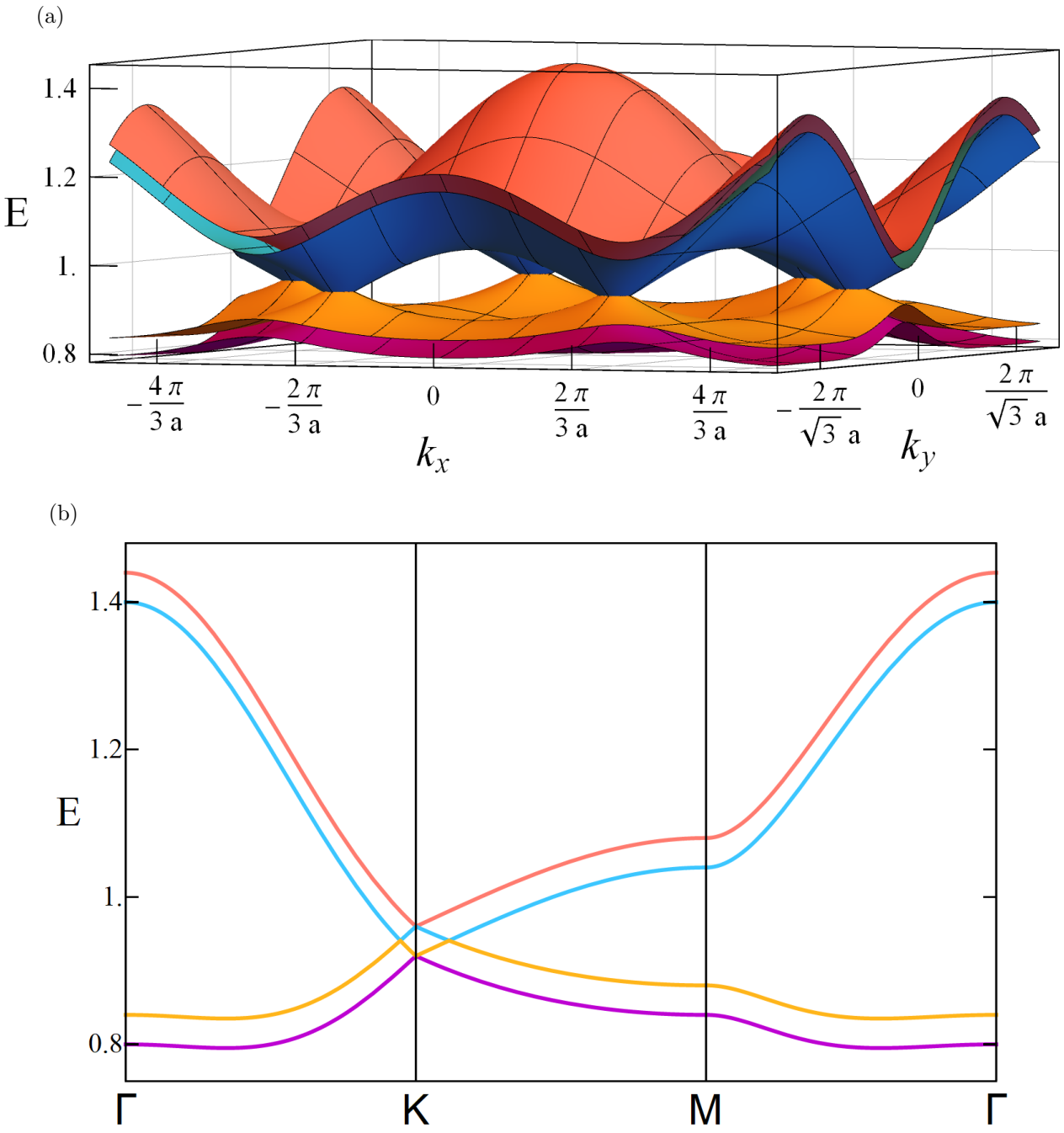

Figure 5: (a) Dispersion relation of bilayer graphene with $A-A$ stacking and next-nearest-neighbor hopping. (b) Dispersion relation as going through the First Brillouin zone by following the path $\Gamma - K - M - \Gamma$. For these panels, the parameter values $\epsilon_0 = 1, t = 0.1, t' = 0.02$ and $t_\perp = 0.02$ were used.

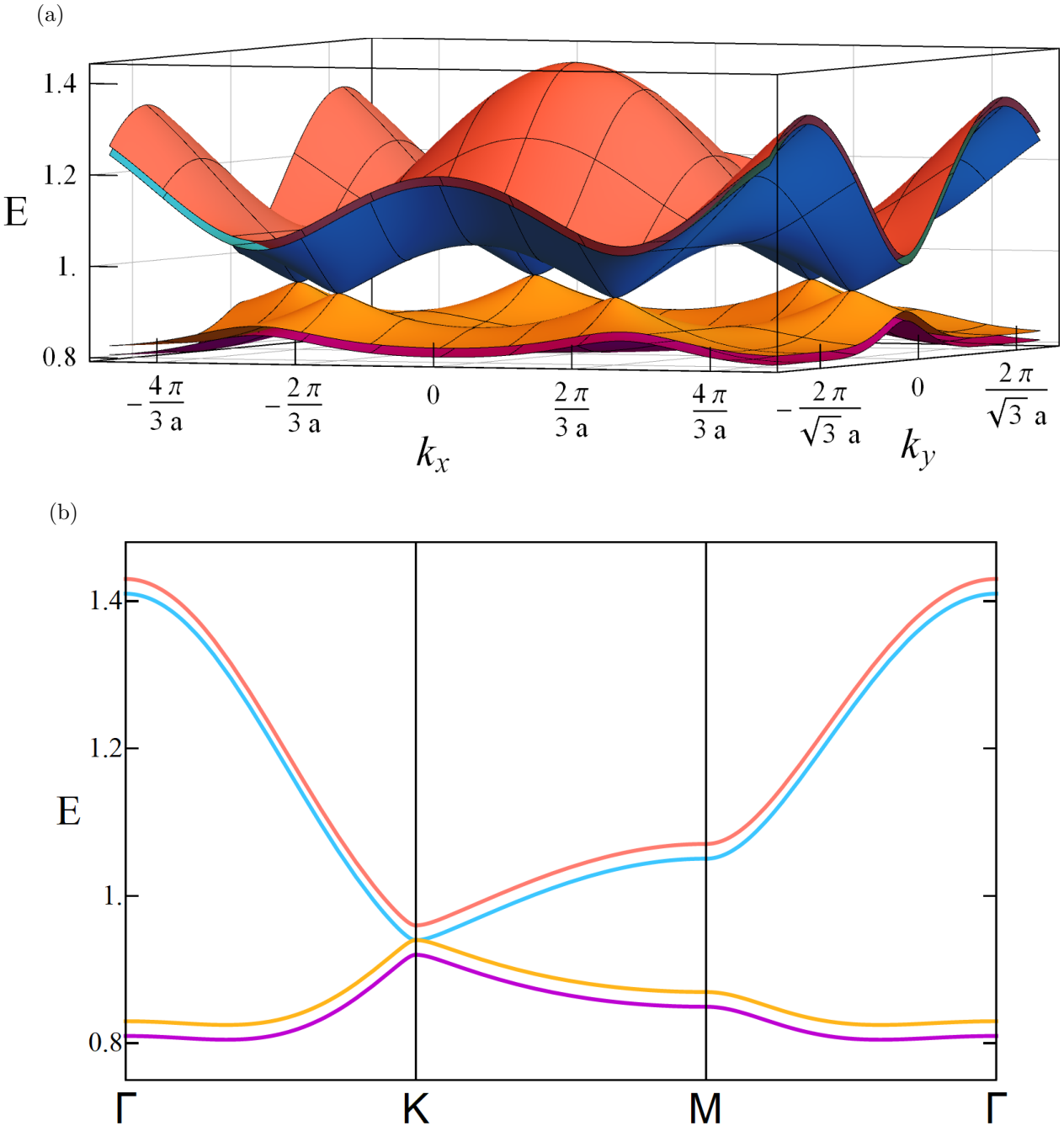

Figure 6: (a) Dispersion relation of bilayer graphene with $A-B$ stacking and next-nearest-neighbor hopping. (b) Dispersion relation as going through the First Brillouin zone by following the path $\Gamma - K - M - \Gamma$. For these panels, the parameter values $\epsilon_0 = 1, t = 0.1, t' = 0.02$ and $t_\perp = 0.02$ were used.

Notice that the dispersion near a K-point in the $A-B$ stacking is quadratic. We will come back to this in Section 3.6 and 4.2. Another important characteristic is that for both stackings, near the M-point, the bands become flat. The diverging density of states there is called a van Hove singularity. As we will discuss in Section 4.2 and 4.3, this can lead to strongly correlated states. However, in bilayer graphene, this flat band is too far above the Fermi energy. A way to lower the flat band to the Fermi energy is by introducting a relative twist between the layers, as we will see in Section 4.2. To discuss the importance of flat bands in dispersion relations, we will first elaborate on the phenomenon of superconductivity. This will be done in the following chapter.

3 Superconductivity

Superconductivity was discovered in 1911 when the Dutch physicist Heike Kamerlingh Onnes whitnessed the vanishing of electrical resistivity in a mercury sample cooled below 4.2K [4,5]. For regular metals, the resistivity gradually declines as the temperature is lowered. For superconductors however, the decline is gradual until a certain critical temperature T_c is reached, at which the resistivity suddenly drops to zero (see Fig. 7a). This observation was substantiated in 1914 when Onnes reported a persisting current in a superconducting ring [53]. During an experiment by Meissner and Ochsenfeld in 1933, it was discovered that superconducting materials expel external magnetic fields [54]. This so-called Meissner-Ochsenfeld effect (see Fig. 7b) is the defining criterion for superconductivity. The first successful theoretical description of it was derived from Maxwell's equations by brothers Heinz and Fritz London in 1935 [55]. The first theory explaining the phenomenology of superconductivity, including its phase transition, is from Ginzburg and Landau [56]. A microscopic description of superconductivity was first given by Bardeen, Cooper and Schrieffer in 1957 [57], for which they recieved the Nobel prize in 1972 [58].

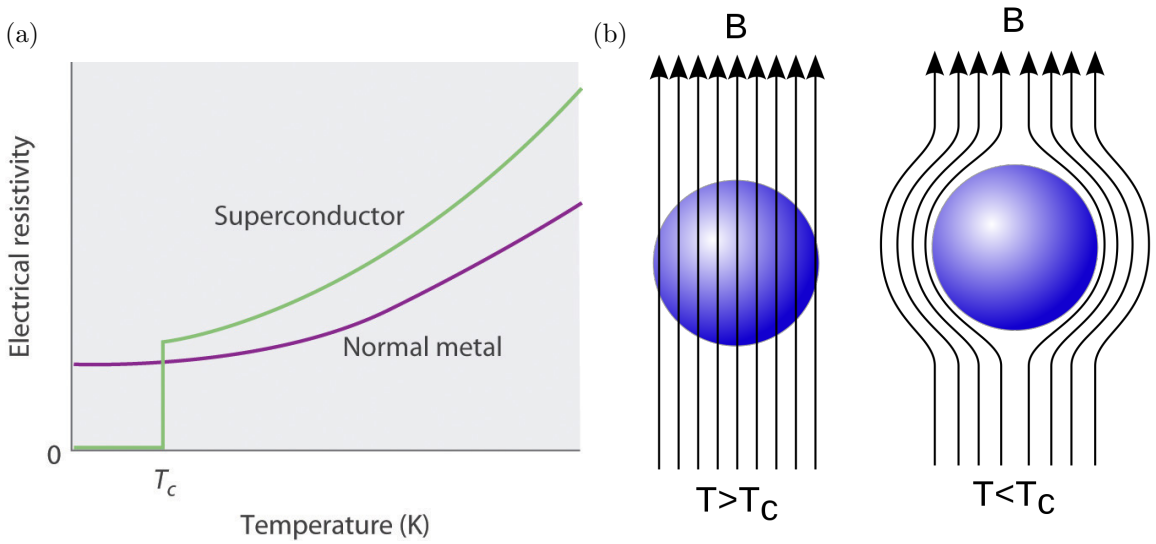

Figure 7: Two typical behaviors of a superconducting material. (a) The electrical resistivity for a superconductor suddenly drops to zero below a certain critical temperature T_c. Panel from Ref. [59]. (b) The Meissner-Ochsenfeld effect. When $T < T_c$, the magnetic field is expelled by the material, which is now in its superconducting state. Panel from Ref. [60].

In Section 3.1, we will discuss the phenomenological theory of superconductivity by reviewing the Ginzburg-Landau theory, leading to the London equation, which explains the Meissner-Ochsenfeld effect. Then, in Section 3.3, we will consider a microscopic approach starting from Cooper pairs and the BCS Hamiltonian, which will be treated using mean-field theory and a Bogoliubov tranformation in Section 3.4. This transformation also alters the form of the wavefunction, as will be discussed in Section 3.5. Finally, we will present the gap equation in Section 3.6, which is the last step towards calculating dispersion relations involving interactions and evaluating the critical temperature T_c.

3.1 Phenomenology of superconductivity

This section is based on Chapter 4 of Ref. [1]. The London equation, describing the current in a superconducting material, can be found using Ginzburg-Landau theory. For this, we let ψ be the order parameter for the superconducting state, and we assume that

$$\begin{aligned} \psi &= 0 \text{ when } T \geq T_c, \\ \psi &\neq 0 \text{ when } T < T_c, \end{aligned} \tag{23}$$

where $\psi = |\psi| e^{i\theta}$ is complex and θ is a constant that is adopted by the system when it goes into its superconducting state (see Fig. 8). By assuming that the order parameter can depend on the position $\vec{r}$, and by including a magnetic field, we can write the free energy as

$$\begin{aligned} F_s(T) = F_n(T) + \int \mathrm{d}\vec{r} \left[\frac{\hbar^2}{2m^*} |(\nabla - \frac{q^* i}{\hbar} \vec{A}) \psi(\vec{r})|^2 + a(T) |\psi(\vec{r})|^2 + b(T) |\psi(\vec{r})|^4 \right] \\ + \frac{1}{2\mu_0} \int \mathrm{d}\vec{r} \vec{B}^2. \end{aligned} \tag{24}$$

Here, F is the free energy and the subscripts s, n denote the superconducting and normal state, respectively; m^* and q^* are the effective mass and charge of the charge carriers, a and b are temperature-dependent functions, where $b \geq 0$ to ensure a stable state, and $\vec{B} = \nabla \times \vec{A}$ is the magnetic field.

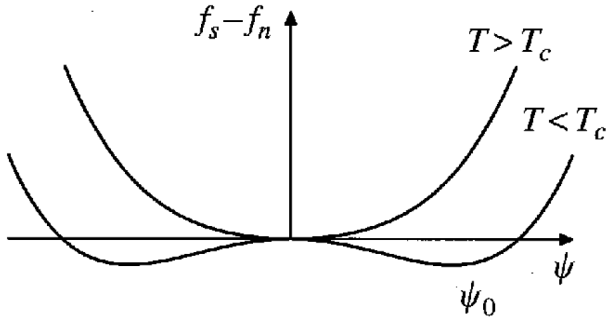

Figure 8: Free energy density difference $f_s - f_n$ between the superconducting and normal state, as a function of the order parameter ψ. A nonzero minimum can be found at ψ_0 when $T < T_c$. Figure from Ref. [1].

Using the Euler-Lagrange equations for ψ^* in Eq. (24) leads to the equation of motion

$$-\frac{\hbar^2}{2m^*} (\nabla - \frac{q^* i}{\hbar} \vec{A})^2 \psi(\vec{r}) + (a + b|\psi(\vec{r})|^2) \psi(\vec{r}) = 0. \tag{25}$$

By extemizing Eq. (24) with respect to $\vec{A}$, we are led to the conserved current,

$$\vec{j} = \frac{q^* i \hbar}{2m^*} [\psi^* (\nabla \psi) - \psi (\nabla \psi^*)] + \frac{(q^*)^2}{m^*} |\psi|^2 \vec{A}. \tag{26}$$

If we assume that $|\psi|$ is constant, then there must be some energy cost associated to changing θ. Under the global phase tranformation $\psi \to \psi e^{i\theta}$, the total energy goes to

$$F_s = F_s^0 + \rho_s \int \mathrm{d}\vec{r} \left(\nabla\theta - \frac{q^* \vec{A}}{\hbar} \right)^2 , \tag{27}$$

with $\rho_s = \hbar^2 |\psi|^2/(2m^*)$ and where F_s^0 is the free energy of the ground state. If we take the functional derivative of this free energy with respect to $\vec{A}$ and assume the ground state (which means θ is constant), we are led to the London equation

$$\vec{j} = -\frac{(q^*)^2}{m^*} |\psi|^2 \vec{A} = -2\rho_s \frac{(q^*)^2}{\hbar^2} \vec{A}. \tag{28}$$

Using the Maxwell equation $\nabla \times \vec{B} = \mu_0 \vec{j}$ and the identity $\vec{B} = \nabla \times \vec{A}$, we can find that

$$\nabla \times (\nabla \times \vec{B}) = -\frac{1}{\lambda^2} \vec{B}, \tag{29}$$

with $\lambda = \sqrt{m^*/(\mu_0 (q^*)^2 |\psi|^2)}$, which has units of length and is called the penetration depth.

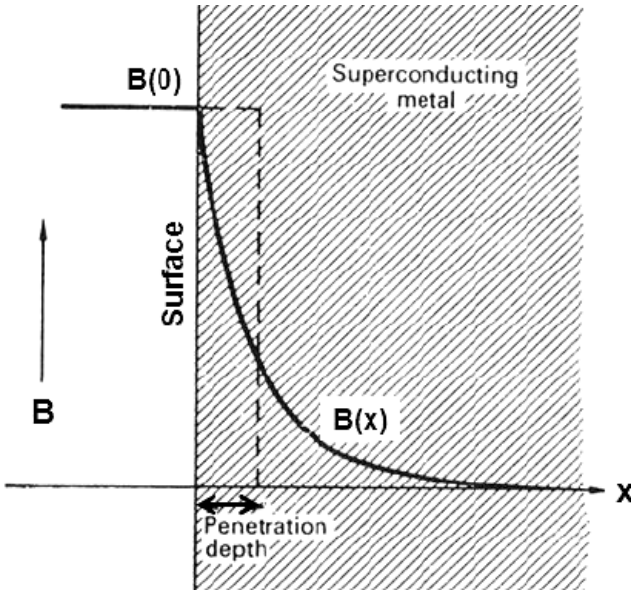

Figure 9: Exponential decay of the magnetic field in a superconducting material. Here, the direction of the $\vec{B}$-field is parallel to the surface of the material. Figure adapted from Ref. [61].

To demonstrate the effect of this equation, consider a surface element of a superconducting material in the $y-z$ plane. The direction of the magnetic field has no perpendicular component near the surface of a superconducting material, so the B_x component will be zero. The strength of the magnetic field however depends only on x, which represents how far we are into the material (see Fig. 9). Hence, we can write that $\vec{B}(x) = \begin{pmatrix} 0 & B_y(x) & B_z(x) \end{pmatrix}^T$. From this we can solve the differential equation (29) to find that $\vec{B}(x) = \vec{B}(0) e^{-x/\lambda}$. When $x = 0$, we are just at the surface. As x increases however, the magnetic field decays exponentially, so in the bulk of the superconducting material the magnetic field is zero. This is called the Meissner-Ochsenfeld effect.

3.2 Cooper pairs

This section is based on Section 6.3 of Ref. [1]. A microscopic approach of superconductivity starts with the assumption that there exists an effective attractive interaction $V = -V_0$ between electrons. It can then be shown that it is energetically more favorable for the electrons to pair up and form a so-called Cooper pair.

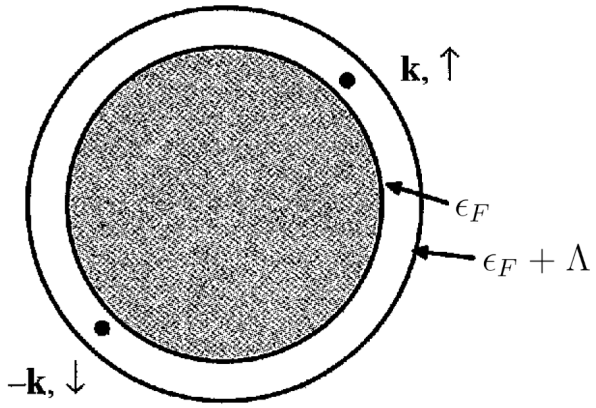

Figure 10: Two electrons with opposite momentum and spin, sitting inside the region between the Fermi surface and the shell with energy $\epsilon_F + \Lambda$. Figure adapted from Ref. [1].

To show this, we will consider a k-space in which all states up to the Fermi surface are filled. Suppose we add two more electrons, with momentum $\vec{k}$ such that $\epsilon_F < \epsilon_{\vec{k}} < \epsilon_F + \Lambda$. Here, Λ is a cutoff energy. If the electrons would pair up, their two-particle wavefunction would be given by

$$\Psi(\vec{r}_1, \sigma_1, \vec{r}_2, \sigma_2) = e^{i\vec{k}\cdot\vec{R}_{cm}} \varphi(\vec{r}_1 - \vec{r}_2) \Phi^{\text{spin}}_{\sigma_1,\sigma_2}, \tag{30}$$

with $\vec{R}_{cm}$ the position of their center of mass. The energy is minimized when the total momentum is zero, that is, when the center of mass does not move. We will assume this ground state from now on. Assume that the spin part of the wavefunction corresponds to a spin singlet

$$\Phi^{\text{spin}}_{\sigma_1,\sigma_2} = \frac{1}{\sqrt{2}}(|\uparrow\downarrow\rangle - |\downarrow\uparrow\rangle). \tag{31}$$

Note that this function is odd under spin exchange, and since the fermionic nature of electrons implies that $\Psi(\vec{r}_1, \sigma_1, \vec{r}_2, \sigma_2) = -\Psi(\vec{r}_2, \sigma_2, \vec{r}_1, \sigma_1)$, this means that $\varphi(\vec{r}_1 - \vec{r}_2)$ is a symmetric function. Now, we will write this part of the wavefunction in terms of Bloch waves

$$\varphi(\vec{r}_1 - \vec{r}_2) = \sum_{\vec{k}} \varphi_{\vec{k}} e^{i\vec{k}\cdot(\vec{r}_1 - \vec{r}_2)}. \tag{32}$$

Note that $\varphi_{\vec{k}} = -\varphi_{\vec{k}}$ because $\varphi(\vec{r}_1 - \vec{r}_2)$ is an even function. We can write a two-particle wavefunction as

$$\Psi(\vec{r}_1, \sigma_1, \vec{r}_2, \sigma_2) = \sum_{\vec{k}} \varphi_{\vec{k}} \begin{vmatrix} \psi_{\vec{k},\uparrow}(\vec{r}_1) & \psi_{-\vec{k},\downarrow}(\vec{r}_1) \\ \psi_{\vec{k},\uparrow}(\vec{r}_2) & \psi_{-\vec{k},\downarrow}(\vec{r}_2) \end{vmatrix}, \tag{33}$$

where $\psi_{\vec{k}}(\vec{r}) = e^{i\vec{k}\cdot\vec{r}}$ is the single-particle Bloch wavefunction. Remember that the sum is restricted to values of $\vec{k}$ for which $\epsilon_F < \epsilon_{\vec{k}} < \epsilon_F + \Lambda$. Putting the two-particle wavefunction into the Schrödinger equation leads to

$$E_{\vec{k}}\varphi_{\vec{k}} = 2\epsilon_{\vec{k}}\varphi_{\vec{k}} - V_0 \sum_{\vec{k}'} \varphi_{\vec{k}'}, \tag{34}$$

with $-V_0$ the attrative interaction. Solving this equation in a self-consistent way, we can find that

$$1 = -V_0 \sum_{\vec{k}} \frac{1}{E_{\vec{k}} - 2\epsilon_{\vec{k}}}. \tag{35}$$

Converting this sum to an integral

$$\sum_{\vec{k}} \frac{1}{E_{\vec{k}} - 2\epsilon_{\vec{k}}} \to \int \mathrm{d}\epsilon \frac{g(\epsilon)}{E - 2\epsilon}, \tag{36}$$

and integrating from ϵ_F to $\epsilon_F + \Lambda$, leads to the energy

$$E = 2\epsilon_F - 2\Lambda \frac{e^{-\frac{1}{\lambda}}}{1 - e^{-\frac{1}{\lambda}}}, \tag{37}$$

with $\lambda = V_0 g(\epsilon_F)/2$ the coupling parameter. Here, we have approximated the density of states $g(\epsilon)$ by the density of states at the Fermi level $g(\epsilon_F)$. The energy of this two-particle wavefunction is lower than $2\epsilon_F$ no matter how small the value of λ, so it is indeed energetically more favorable for electrons to form bound states with opposite momentum and spin, which are called Cooper pairs.

3.3 Attractive effective electron-electron interaction

This section is based on Section 6.2 of Ref. [1] and Section 3.7 of Ref. [3]. One might wonder if an effective attractive electron-electron interaction exists at all because of the repulsive Coulomb interaction

$$V(\vec{r} - \vec{r}') = \frac{e^2}{4\pi\epsilon_0 |\vec{r} - \vec{r}'|}, \tag{38}$$

with ϵ_0 the vacuum permittivity. In a crystal, this interaction is reduced by screening effects. This can be included in the Coulomb interaction by inserting the Thomas-Fermi approximation into Poisson's equation, which leads to

$$V(\vec{r} - \vec{r}') = \frac{e^2}{4\pi\epsilon_0 |\vec{r} - \vec{r}'|} e^{-\frac{|\vec{r} - \vec{r}'|}{r_{TF}}}, \tag{39}$$

where r_{TF} is the Thomas Fermi screening length. The exponential decay of the repulsive interaction gives room for a phonon-mediated (see Fig. 11) effective attractive electron-electron interaction.

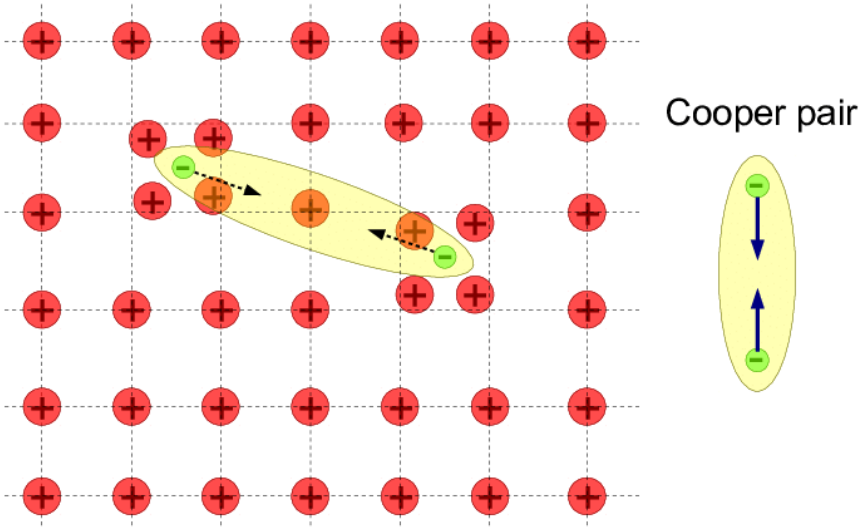

Figure 11: Visualisation of a Cooper pair. The distortion of the ion lattice around an electron causes a local excess of positive charge. This attracts another electron, leading to the formation of a Cooper pair. The formation of Cooper pairs can thus be seen as an exchange interaction between electrons and lattice excitations (phonons) [62]. Figure from Ref. [62].

Consider the electron-phonon Hamiltonian

$$\mathcal{H}_{e-ph} = \sum_{\vec{k},\vec{q},s,\sigma} W_{\vec{q},s} c^\dagger_{\vec{k}+\vec{q},\sigma} c_{\vec{k},\sigma} \left[a_s(\vec{q}) + a^\dagger_s(-\vec{q})\right], \tag{40}$$

where $a^\dagger$ and a are the phonon creation and annihilation operators with mode s, $\vec{q}$ represents the transferred momentum between an electron and a phonon upon interaction, and $W_{\vec{q},s}$ is a measure for the energy associated to this interaction. This Hamiltonian arises from the electron-lattice Hamiltonian $H_{e-l} = \int \mathrm{d}\vec{x} \frac{1}{N} \sum_{\vec{R}_i} \rho(\vec{x}) V(\vec{x} - \vec{X}_i)$, where ρ is the electron density, $\vec{X}_i = \vec{R}_i + \vec{r}_i$ is the location of atom i with equilibrium $\vec{R}_i$ and deviation $\vec{r}_i$, and V is the potential that the electrons feel due to the atoms. The electron-phonon Hamiltonian can be found by taking the first order of the Taylor expansion of H_{e-l} in $\vec{r}_i$ (note that the zero'th order leads to the tight-binding model). Using the definition of the ladder operators, we can find the displacement of the atoms

$$\delta\vec{R}_i = \sum_{\vec{q},s} \hat{e}_{\vec{q}s} \sqrt{\frac{\hbar}{2M\omega_{\vec{q}s}}} (a^\dagger_{\vec{q}s} + a_{\vec{q}s}) e^{i\vec{q}\cdot\vec{R}_i}. \tag{41}$$

This deplacement will cause a deformation of the potential V such that

$$\delta V(\vec{r}) = \sum_i \frac{\partial V(\vec{r})}{\partial \vec{R}_i} \delta\vec{R}_i. \tag{42}$$

Because of this deformation, an electron with wavevector $\vec{k}_1$ may scatter to a state with wavevector $\vec{k}_1 - \vec{q}$. In doing so, a phonon of momentum $\vec{q}$ is created. After some time, this

phonon will be absorbed by another electron that was in a state with wavevector $\vec{k}_2$, such that it now has wavevector $\vec{k}_2 + \vec{q}$. Effectively, we can see this as an interaction between the two electrons where one of them has transferred a momentum of $\vec{q}$ to the other one. When performing a second-order perturbation theory calculation, it can be found that the effective interaction can be described by

$$V(\vec{q}, \omega) = |g_{\vec{q}s}|^2 \frac{\omega_{\vec{q}s}}{\omega^2 - \omega_{\vec{q}s}^2}. \tag{43}$$

This $g_{\vec{q}s}$ is of order $\sqrt{m/M}$, with m the effective mass of an electron at the Fermi surface and M the mass of an ion [63]. Since m/M is typically of order 10^{-4}, the electrons and phonons are only weakly coupled. Therefore, it is justified to only take into account the basic scattering principle as described above and we do not need to include scatterings of higher order.

This effective potential is too complicated for analytical calculations. Therefore, we will simplify it by neglecting the dependence on $\vec{q}$. The frequency $\omega_{\vec{q}s}$ is then replaced by the Debye frequency ω_D, and the interaction vertex $g_{\vec{q}s}$ is set to a constant g_{eff}. This yields

$$V(\omega) = |g_{\text{eff}}|^2 \frac{\omega_D}{\omega^2 - \omega_D^2}. \tag{44}$$

For $\omega < \omega_D$, we can see that this interaction is attractive. We can simplify the potential even further by limiting ourselves to the interesting region $\pm k_B T$ away from the Fermi energy, and assuming that $\hbar\omega_D \gg k_B T$ (this is the temperature of interest for superconductivity). This leads to the simplest form of the potential

$$V = -\frac{|g_{\text{eff}}|^2}{\omega_D} = -V_0, \tag{45}$$

with the corresponding effective Hamiltonian for the effective electron-electron interaction being

$$\mathcal{H} = V \sum_{\substack{\vec{k}_1, \vec{k}_2, \vec{q} \\ \sigma_1, \sigma_2}} c^\dagger_{\vec{k}_1 - \vec{q}, \sigma_1} c^\dagger_{\vec{k}_2 + \vec{q}, \sigma_2} c_{\vec{k}_2, \sigma_2} c_{\vec{k}_1, \sigma_1}, \tag{46}$$

with the restriction $|\epsilon_{\vec{k}_i} - \epsilon_F| < \hbar\omega_D$. With this we have a description for the interactions between electrons that occupy states near the Fermi surface.

3.4 Mean-field Hamiltonian

This section is based on Section 3.1 of Ref. [64]. We will consider a Hamiltonian that includes the kinetic energy of the electrons and an interaction term that only involves Cooper pairs. Here, we will assume an interaction that may depend on the transferred momentum, but in Section 3.6 we will insert an effective value as we have seen in the previous two sections. This leads to the Hamiltonian

$$\mathcal{H} = \sum_{\vec{k}, \sigma} \epsilon_{\vec{k}} c^\dagger_{\vec{k}, \sigma} c_{\vec{k}, \sigma} + \frac{1}{2} \sum_{\vec{k}, \vec{k}', \sigma} V_{\vec{k}\vec{k}'} c^\dagger_{\vec{k}, \sigma} c^\dagger_{-\vec{k}, -\sigma} c_{-\vec{k}', -\sigma} c_{\vec{k}', \sigma}, \tag{47}$$

where the factor $1/2$ is there to prevent overcounting the pairs. We will treat this Hamiltonian using the mean-field approximation

$$\begin{aligned} c^\dagger_{\vec{k},\sigma} c^\dagger_{-\vec{k},-\sigma} c_{-\vec{k}',-\sigma} c_{\vec{k}',\sigma} \approx \langle c^\dagger_{\vec{k},\sigma} c^\dagger_{-\vec{k},-\sigma} \rangle \, c_{-\vec{k}',-\sigma} c_{\vec{k}',\sigma} + \\ c^\dagger_{\vec{k},\sigma} c^\dagger_{-\vec{k},-\sigma} \langle c_{-\vec{k}',-\sigma} c_{\vec{k}',\sigma} \rangle - \\ \langle c^\dagger_{\vec{k},\sigma} c^\dagger_{-\vec{k},-\sigma} \rangle \langle c_{-\vec{k}',-\sigma} c_{\vec{k}',\sigma} \rangle. \end{aligned} \tag{48}$$

Notice that using this approximation, the Hamiltonian has terms like $c^\dagger c^\dagger$ and cc, which do not conserve the amount of particles in the system. Therefore, we will make a Bogoliubov transformation, which is a change of basis such that the vacuum is redefined to be the ground state of the BCS wavefunction (see appendix D). This transformation is given by

$$\begin{aligned} \gamma_{\vec{k},\uparrow} &= u_{\vec{k}} c_{\vec{k},\uparrow} - v_{\vec{k}} c^\dagger_{-\vec{k},\downarrow}, \\ \gamma^\dagger_{-\vec{k},\downarrow} &= u^*_{\vec{k}} c^\dagger_{-\vec{k},\uparrow} + v^*_{\vec{k}} c_{\vec{k},\uparrow}, \end{aligned} \tag{49}$$

where the $u_{\vec{k}}, v_{\vec{k}}$ are complex parameters that depend on $\vec{k}$. The Bogoliubov creation and annihalition operators $\gamma^\dagger$ and γ, respectively, create and destroy quasiparticles called Bogoliubons, which are a combination of an electron and a hole. By imposing $|u_{\vec{k}}|^2 + |v_{\vec{k}}|^2 = 1$, the Bogoliubov operators satisfy the fermionic anticommutation relations,

$$\begin{aligned} \{\gamma^\dagger_{\vec{k},\sigma}, \gamma_{\vec{k}',\sigma'}\} &= \delta_{\vec{k},\vec{k}'} \delta_{\sigma,\sigma'}, \\ \{\gamma_{\vec{k},\sigma}, \gamma_{\vec{k}',\sigma'}\} &= 0, \\ \{\gamma^\dagger_{\vec{k},\sigma}, \gamma^\dagger_{\vec{k}',\sigma'}\} &= 0. \end{aligned} \tag{50}$$

The electron creation and annihilation operators can be written in terms of the Bogoliubov operators as

$$\begin{aligned} c_{\vec{k},\uparrow} &= u^*_{\vec{k}} \gamma_{\vec{k},\uparrow} + v_{\vec{k}} \gamma^\dagger_{-\vec{k},\downarrow}, \\ c^\dagger_{-\vec{k},\downarrow} &= u_{\vec{k}} \gamma^\dagger_{-\vec{k},\downarrow} - v^*_{\vec{k}} \gamma_{\vec{k},\uparrow}. \end{aligned} \tag{51}$$

If we now write

$$\Delta_{\vec{k}} = \frac{1}{N} \sum_{\vec{k}'} V_{\vec{k}\vec{k}'} \langle c_{-\vec{k}',\downarrow} c_{\vec{k}',\uparrow} \rangle, \tag{52}$$

and impose one more constraint,

$$2\epsilon_{\vec{k}} u_{\vec{k}} v_{\vec{k}} + \Delta_{\vec{k}} u^2_{\vec{k}} - \Delta^*_{\vec{k}} v^2_{\vec{k}} = 0, \tag{53}$$

in order to prevent the existence of terms like $\gamma^\dagger \gamma^\dagger$ and $\gamma\gamma$ in the Hamiltonian, it can be found that

$$\begin{aligned} \frac{v_{\vec{k}}}{u_{\vec{k}}} &= \frac{\epsilon_{\vec{k}} - \sqrt{(\epsilon_{\vec{k}})^2 + |\Delta_{\vec{k}}|^2}}{\Delta^*_{\vec{k}}}, \\ |u_{\vec{k}}|^2 &= \frac{1}{2}\left(1 + \frac{\epsilon_{\vec{k}}}{\sqrt{(\epsilon_{\vec{k}})^2 + |\Delta_{\vec{k}}|^2}}\right), \\ |v_{\vec{k}}|^2 &= \frac{1}{2}\left(1 - \frac{\epsilon_{\vec{k}}}{\sqrt{(\epsilon_{\vec{k}})^2 + |\Delta_{\vec{k}}|^2}}\right). \end{aligned} \tag{54}$$

The Hamiltonian can then be written as

$$\mathcal{H} = \sum_{\vec{k}} E_{\vec{k}}(\gamma^\dagger_{\vec{k},\uparrow}\gamma_{\vec{k},\uparrow} + \gamma^\dagger_{-\vec{k},\downarrow}\gamma_{-\vec{k},\downarrow}) + E_{BCS}, \tag{55}$$

where $E_{\vec{k}} = \sqrt{(\epsilon_{\vec{k}})^2 + |\Delta_{\vec{k}}|^2}$ is the dispersion of the Bogoliubons, and the energy of the vacuum is defined as $E_{BCS} = \sum_{\vec{k}} \left[\left(\epsilon_{\vec{k}} + E_{\vec{k}}\right) - \sum_{\vec{k}'} \Delta^*_{\vec{k}} V^{-1}_{\vec{k}\vec{k}'} \Delta_{\vec{k}'} \right]$. The system can now be treated as a free fermion gas of Bogoliubons.

3.5 Cooper pair wavefunction

This section is based on Section 6.4 of Ref. [1]. The vacuum of the Bogoliubons is given by the ground state BCS wavefunction $|\Psi_{BCS}\rangle$, such that $\gamma_{\vec{k},\sigma}|\Psi_{BCS}\rangle = 0$. We will now show how this ground state can be written in terms of the original vacuum $|0\rangle$. By filling in the definition of the Bogoliubon annihilation operator, we get

$$u_{\vec{k}} c_{\vec{k},\uparrow}|\Psi_{BCS}\rangle = v_{\vec{k}} c^\dagger_{-\vec{k},\downarrow}|\Psi_{BCS}\rangle. \tag{56}$$

The BCS wavefunction is made up of Cooper pairs and has the form

$$|\Psi_{BCS}\rangle = C e^{\sum_{\vec{q}} \alpha_{\vec{q}} P^\dagger_{\vec{q}}}|0\rangle, \tag{57}$$

as proposed by Schrieffer [57], where $P^\dagger_{\vec{k}} = c^\dagger_{\vec{k},\uparrow} c^\dagger_{-\vec{k},\downarrow}$ and $P_{\vec{k}} = c_{\vec{k},\uparrow} c_{-\vec{k},\downarrow}$ are the Cooper pair creation and annihilation operators, respectively, C is a normalization constant, and $\alpha_{\vec{k}}$ is a function still to be determined.

Using the commutation relation $[P^\dagger_{\vec{k}}, P^\dagger_{\vec{k}'}] = 0$, we can take the sum out of the exponential and write it as a product

$$|\Psi_{BCS}\rangle = C \prod_{\vec{q}} e^{\alpha_{\vec{q}} P^\dagger_{\vec{q}}}|0\rangle. \tag{58}$$

Now, using $(P^\dagger_{\vec{k}})^2 = 0$, we can Taylor expand the exponential to find

$$|\Psi_{BCS}\rangle = C \prod_{\vec{q}} (1 + \alpha_{\vec{q}} P^\dagger_{\vec{q}})|0\rangle. \tag{59}$$

Assume for now that we only have one single Cooper pair, with $\vec{q} = \vec{k}$. Using Eq. (56), this leads to

$$u_{\vec{k}} c_{\vec{k},\uparrow}|\Psi_{BCS}\rangle = u_{\vec{k}} c_{\vec{k},\uparrow}(1 + \alpha_{\vec{k}} P^\dagger_{\vec{k}})|0\rangle = v_{\vec{k}} c^\dagger_{-\vec{k},\downarrow}(1 + \alpha_{\vec{k}} P^\dagger_{\vec{k}})|0\rangle = v_{\vec{k}} c^\dagger_{-\vec{k},\downarrow}|\Psi_{BCS}\rangle. \tag{60}$$

Notice that $c_{\vec{k},\uparrow}|0\rangle$ and $c^\dagger_{-\vec{k},\downarrow} P^\dagger_{\vec{k}}|0\rangle$ are equal to zero, reducing Eq. (60) to

$$u_{\vec{k}} \alpha_{\vec{k}} c^\dagger_{-\vec{k},\downarrow}|0\rangle = v_{\vec{k}} c^\dagger_{-\vec{k},\downarrow}|0\rangle, \tag{61}$$

which implies that $\alpha_{\vec{k}} = v_{\vec{k}}/u_{\vec{k}}$. The normalization constant can be found by filling in $\langle \Psi_{BCS} | \Psi_{BCS} \rangle = 1$, which leads to

$$C = \prod_{\vec{k}} \frac{1}{\sqrt{1 + |\alpha_{\vec{k}}|^2}}. \tag{62}$$

If we insert Eq. (62) in Eq. (59), we get the convenient form

$$|\Psi_{BCS}\rangle = \prod_{\vec{k}} (u_{\vec{k}} + v_{\vec{k}} P^\dagger_{\vec{k}}) \, |0\rangle. \tag{63}$$

3.6 Gap equation

This section is based on Section 3.2 of Ref. [64]. Writing out the expression for $\Delta_{\vec{k}}$ in terms of the Bogoliubov operators, we find

$$\begin{aligned} \Delta_{\vec{k}} &= -\frac{1}{N} \sum_{\vec{k}'} V_{\vec{k}\vec{k}'} \, \langle c_{-\vec{k}',\downarrow} c_{\vec{k}',\uparrow} \rangle = \\ &= -\frac{1}{N} \sum_{\vec{k}'} V_{\vec{k}\vec{k}'} v_{\vec{k}'} u^*_{\vec{k}'} \big(\, \langle \gamma_{-\vec{k},\downarrow} \gamma^\dagger_{-\vec{k},\downarrow} \rangle - \langle \gamma^\dagger_{\vec{k},\uparrow} \gamma_{\vec{k},\uparrow} \rangle \, \big) \end{aligned} \tag{64}$$

Because the Bogoliubov operators are fermionic, the expectation value of the Bogoliubon particle number follows the Fermi-Dirac distribution, such that

$$\langle \gamma^\dagger_{\vec{k},\uparrow} \gamma_{\vec{k},\uparrow} \rangle = \langle \gamma^\dagger_{-\vec{k},\downarrow} \gamma_{-\vec{k},\downarrow} \rangle = \frac{1}{e^{\beta E_{\vec{k}}} + 1}, \tag{65}$$

where $E_{\vec{k}} = \sqrt{(\epsilon_{\vec{k}})^2 + |\Delta_{\vec{k}}|^2}$. Then

$$\langle \gamma_{-\vec{k},\downarrow} \gamma^\dagger_{-\vec{k},\downarrow} \rangle - \langle \gamma^\dagger_{\vec{k},\uparrow} \gamma_{\vec{k},\uparrow} \rangle = 1 - \frac{2}{e^{\beta E_{\vec{k}}} + 1} = \frac{e^{\beta E_{\vec{k}}} - 1}{e^{\beta E_{\vec{k}}} + 1} = \tanh\left(\frac{1}{2} \beta E_{\vec{k}} \right), \tag{66}$$

which leads to

$$\Delta_{\vec{k}} = -\frac{1}{N} \sum_{\vec{k}'} \frac{V_{\vec{k}\vec{k}'} \Delta_{\vec{k}'}}{2 E_{\vec{k}'}} \tanh\left(\frac{1}{2} \beta E_{\vec{k}'} \right). \tag{67}$$

Now, assume that $V_{\vec{k}\vec{k}'} = -V_0$ and $\Delta_{\vec{k}} = \Delta_0$ are independent of $\vec{k}$. This corresponds to the assumption that the interaction is a constant effective attractive interaction (as done in 3.2), and that the spin part of the wavefunction corresponds to a spin singlet (as done in 3.3). At this point, we will introduce the chemical potential μ such that $\epsilon_{\vec{k}} \to \epsilon_{\vec{k}} - \mu$. The previous can then be written as

$$1 = \frac{1}{N} \sum_{\vec{k}} \frac{V_0}{2\sqrt{(\epsilon_{\vec{k}} - \mu)^2 + |\Delta_0|^2}} \tanh\left(\frac{1}{2} \beta \sqrt{(\epsilon_{\vec{k}} - \mu)^2 + |\Delta_0|^2} \right). \tag{68}$$

Converting this into an integral yields

$$\frac{2N}{V_0} = \int_{\vec{k}} \mathrm{d}\vec{k} \frac{g(\vec{k})}{\sqrt{(\epsilon_{\vec{k}} - \mu)^2 + |\Delta_0|^2}} \tanh\left(\frac{1}{2}\beta\sqrt{(\epsilon_{\vec{k}} - \mu)^2 + |\Delta_0|^2}\right), \tag{69}$$

where $g(\vec{k})$ is the density of states in k-space. Notice that

$$\begin{aligned} g(k)\mathrm{d}k &= \frac{N}{V_{BZ}} \int_k^{k+\mathrm{d}k} k^{d-1}\mathrm{d}k \int_\theta^{2\pi} \mathrm{d}\theta \prod_{n=1}^{d-2} \int_0^\pi \sin^{d-1-n}(\phi_n)\mathrm{d}\phi_n = \\ &\approx \frac{NI}{V_{BZ}} k^{d-1}\mathrm{d}k, \end{aligned} \tag{70}$$

where $I = \int_\theta^{2\pi} \mathrm{d}\theta \prod_{n=1}^{d-2} \int_0^\pi \sin^{d-1-n}(\phi_n)\mathrm{d}\phi_n = 2\pi^{d/2}/(\Gamma(d/2))$. Now, we add a small original contribution to this calculation. Suppose that the dispersion has the generic form $\epsilon(\vec{k}) = \mu + Ck^\alpha$. Then, $\mathrm{d}k/\mathrm{d}\epsilon = (C\alpha k^{\alpha-1})^{-1}$, such that

$$g(\epsilon) = g(k)\frac{\mathrm{d}k}{\mathrm{d}\epsilon} = \frac{NI}{\alpha V_{BZ} C^{\frac{d}{\alpha}}} (\epsilon - \mu)^{\frac{d}{\alpha}-1}. \tag{71}$$

The equality then becomes

$$\frac{\alpha V_{BZ} C^{\frac{d}{\alpha}}}{IV_0} = \int_\mu^{\mu+\hbar\omega_D} \mathrm{d}\epsilon \frac{(\epsilon - \mu)^{\frac{d}{\alpha}-1}}{\sqrt{(\epsilon - \mu)^2 + |\Delta_0|^2}} \tanh\left(\frac{1}{2}\beta\sqrt{(\epsilon - \mu)^2 + |\Delta_0|^2}\right). \tag{72}$$

With this equation, we can find the critical potential for superconductivity by letting $\Delta_0 \to 0, T \to 0$. In this limit,

$$\frac{\alpha V_{BZ} C^{\frac{d}{\alpha}}}{IV_c} = \int_\mu^{\mu+\hbar\omega_D} \mathrm{d}\epsilon (\epsilon - \mu)^{\frac{d}{\alpha}-2} = \begin{cases} \frac{1}{\frac{d}{\alpha}-1}(\hbar\omega_D)^{\frac{d}{\alpha}-1} & \text{if } \frac{d}{\alpha} \neq 1, \\ \ln(\hbar\omega_D) - \ln(0) & \text{if } \frac{d}{\alpha} = 1. \end{cases} \tag{73}$$

This means that

$$V_c = (d - \alpha)\frac{V_{BZ} C^{\frac{d}{\alpha}}}{I(\hbar\omega_D)^{\frac{d}{\alpha}-1}} \quad \text{for } \frac{d}{\alpha} \neq 1. \tag{74}$$

Notice that there is a divergence in Eq. (73) for the case that $d/\alpha = 1$, which implies that $V_c \to 0$. The critical temperature can be calculated by taking the limit $\Delta_0 \to 0$ in Eq. (72) provided that $V_0 > V_c$ ($V_0 = V_c$ will lead to $T_c \to 0$). This leads to the numerically solvable integral equation

$$\frac{\alpha V_{BZ} C^{\frac{d}{\alpha}}}{IV_0} = \int_0^{\hbar\omega_D} \mathrm{d}\epsilon \epsilon^{\frac{d}{\alpha}-2} \tanh\left(\frac{\epsilon}{2k_B T_c}\right). \tag{75}$$

For $d/\alpha = 1$ however, the integral diverges, so there will be no solution for the critical temperature. This means that, using this approach, we cannot see superconductivity when $d/\alpha = 1$. This is the reason that we do not see superconductivity in $A-B$ stacked graphene for $T > 0$. In the case of graphene, we have $d = 2, \alpha = 1, C = \hbar v_F, I = 2\pi$ and $V_{BZ} = 8\pi^2/(\sqrt{3}a^2)$. The critical potential can be recognized in Fig. 12 by the nonzero solution for Δ_0 of Eq. (67) when $V_0 > V_c$. If V_0 is increased beyond V_c, the value of the critical temperature is affected, as can be seen in Fig. 13. For graphene, V_c is too high to see superconductivity [65].

When calculating the gap equation, one usually approximates the density of states $g(\epsilon)$ by the density of states at the Fermi level $g(\epsilon_F)$. In this section however, we have assumed a general dispersion in arbitrary dimension, leading to a gap equation for generic d and α. This means that this derivation also holds for fractional dimensions, and could thus be used to describe superconductivity in fractals. This result has not been found in literature, so we think that this may be an original contribution.

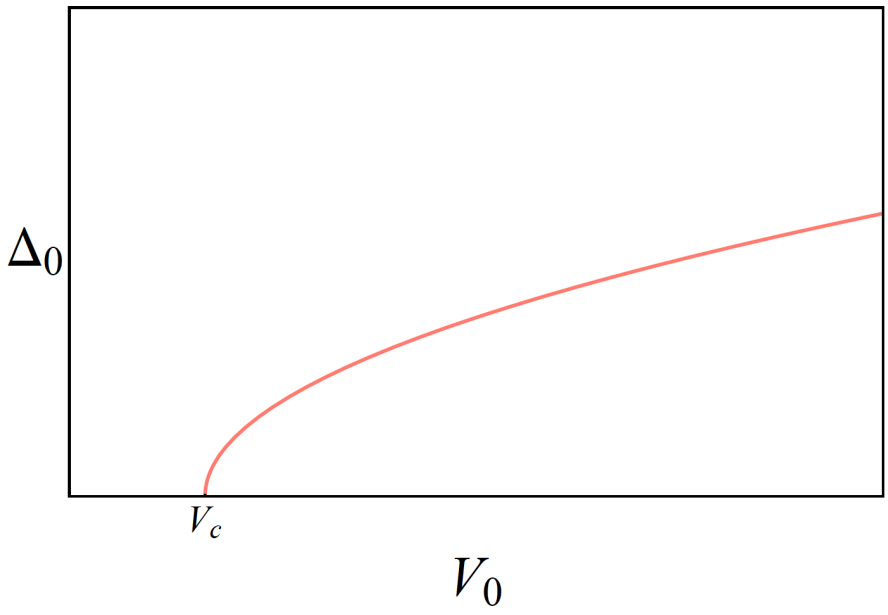

Figure 12: Plot of Δ_0 against the potential V_0 with critical potential V_c for graphene in the limit that $T \to 0$.

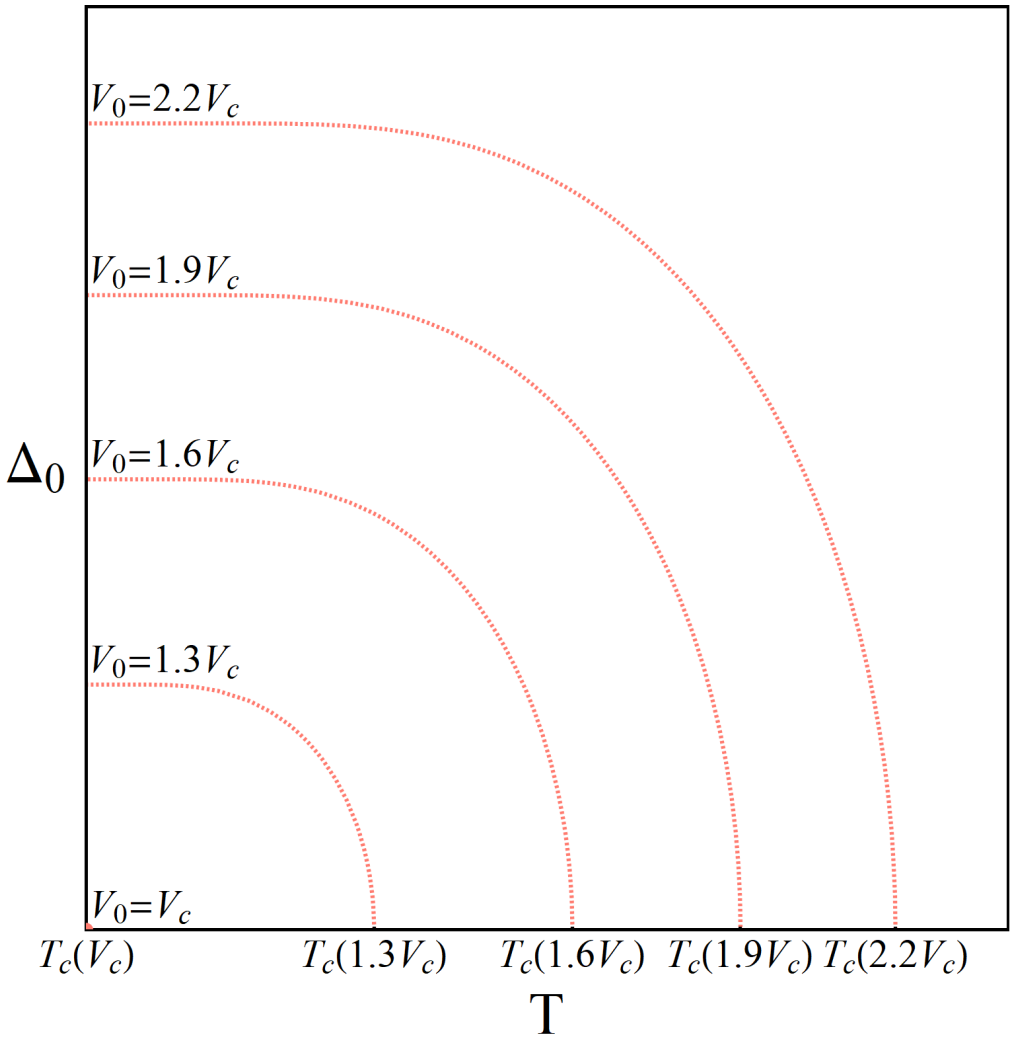

Figure 13: Plot of Δ_0 as a function of the temperature for multiple values of V_0 for graphene. The critical temperatures for the different V_0 are indicated by T_c. The shape of the graphs is universal up to the spacing between the contours.

4 Twisted bilayer graphene

Twisted bilayer graphene is a bilayer of graphene with a relative twist between the layers. When introducing this twist, a superstructure called a Moiré pattern [66, 67] emerges, as can be seen in Fig. 14. A Moiré pattern is an interference pattern that emerges when two (not necessarily periodic) structures are superposed [67]. The name for this type of pattern originates from the French word *moire*, a type of textile with a rippled appearance that is created by passing two dampened layers of fabric between two hot cilinders [68]. Originally, the fabric used in this procedure was silk, and it's wavy appearance gave moiré treated silk the name *watered silk* [69]. Moire was formerly worn by the upper class and can nowadays still be seen in some gowns [70–72].

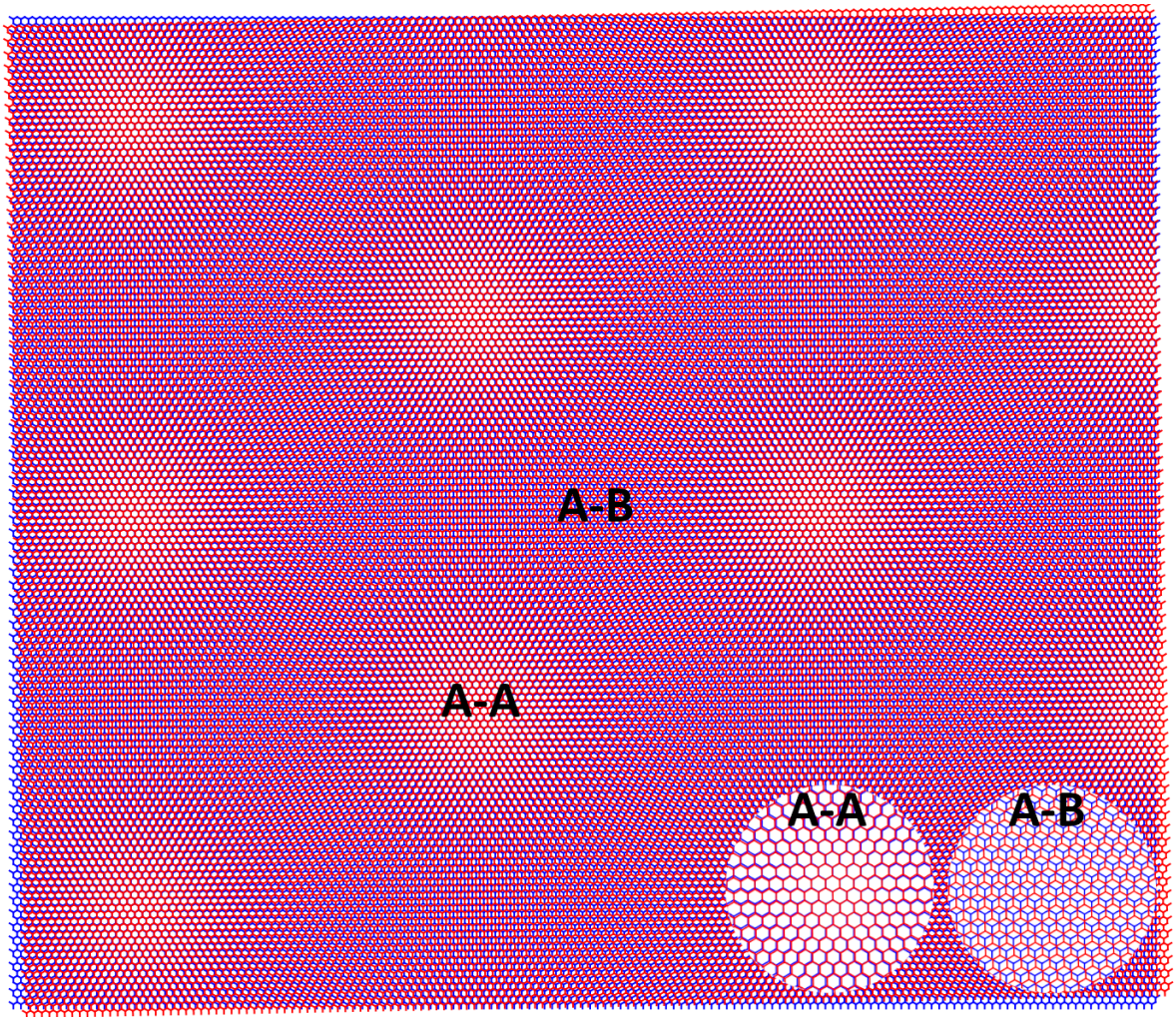

Figure 14: Twisted bilayer graphene for a twist angle of 1.1°. An $A-B$ stacking was assumed before twisting. The Moiré pattern[1] consists of locally $A-A$ stacked spots and locally $A-B$ stacked spots, as indicated in the picture. Enlarged views of the local stackings are shown in the insets in the bottom right corner.

[1]If you are seeing this picture on a computer, you may notice some straight lines appearing depending on your zoom level. This is actually another Moiré pattern that is formed by the pixels on your screen! This is also the reason why you should not wear stripes if you appear on TV.

In physics, Moiré patterns are often used to measure surface deformations of materials (for example due to thermal expansion). This is done by engraving or projecting a grating on the surface of the material to be studied, and introducing a reference grating [73]. The superposition of the two will then produce a Moiré pattern. If the material is subject to some strain, it will deform or displace, thus changing the surface. This gives rise to a change in the Moiré pattern, which can then be studied [73, 74]. Microelectronic devices are an example of the importance of such measurements: since these electronic devices are very small, the temperature-induced stresses on components with different thermal expansion rates become relevant and need to be taken into account to create a well-functioning device [75].

In this chapter, we review for which twist angles a periodic Moiré superlattice can be achieved, and present the corresponding lattice vectors in Section 4.1. In Section 4.2, we exploit the periodicity of the Moiré pattern and derive the dispersion relation for tBLG. In Section 4.3, we discuss the similarities and differences between tBLG and high-T_c cuprates in relation to their phase diagrams.

4.1 Lattice vectors of the Moiré pattern

This section is based on Ref. [76]. In order to find the primitive vectors for the Moiré supercells, we lay the origin on the rotation center and characterize the vectors indicating lattice positions from there. Recall from Section 2.1 that the lattice vectors of an unrotated layer are given by $\vec{a}_1$ and $\vec{a}_2$. Assuming an $A-B$ stacking prior to twisting, we have that $\vec{r}_{\mathrm{hc1}}(m,n) = \vec{r}_{B2}(m,n) = m\vec{a}_1 + n\vec{a}_2$, such that the rotation center (corresponding to $m = n = 0$) coincides with a honeycomb cell center of the first (bottom) layer $\vec{r}_{\mathrm{hc1}}$ and a B-type site of the second (top) layer $\vec{r}_{B2}$ (see Fig. 15). If we twist the top layer with respect

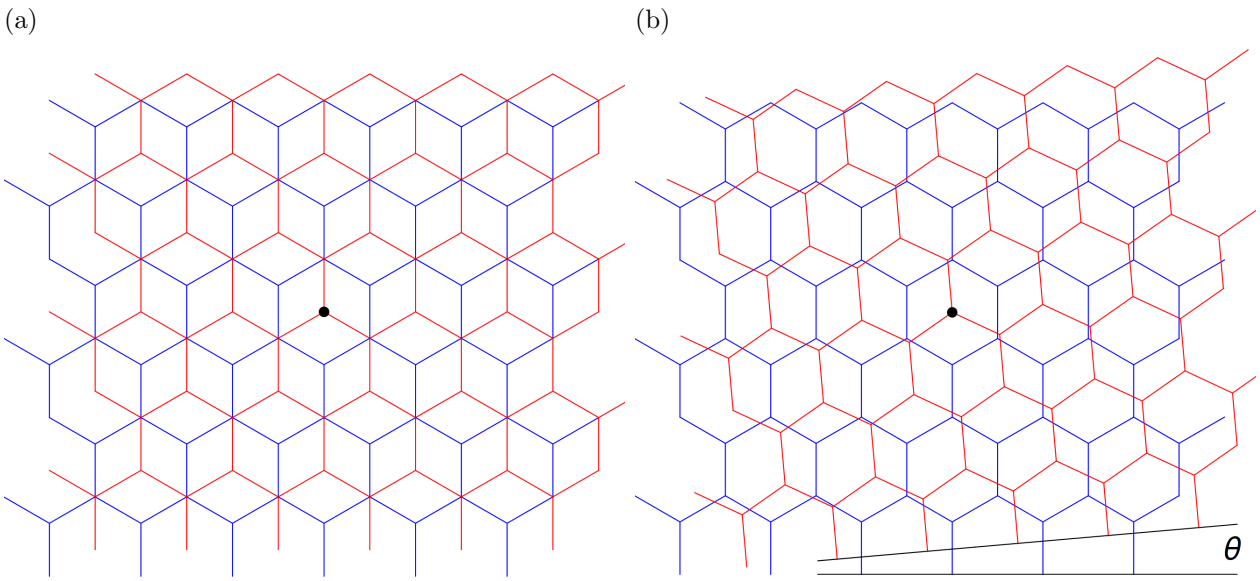

Figure 15: Twisted bilayer graphene. The top layer (in red) is twisted around the black dot. (a) Before twisting. (b) After twisting with angle θ.

to the bottom one, then the only way that a commensurate structure can be achieved is by rotating a B-site of the second layer to a honeycomb cell center of the first layer. If we restrict the twist angle to the domain $[-\pi/6, \pi/3]$ and denote such a B-site by $\vec{P} = n\vec{a}_1 + m\vec{a}_2$ where $n > m > 0$ without loss of generality, then there are two rotations possible to end up in a honeycomb cell center of the first layer. These points are denoted by

$$\begin{aligned} \vec{Q}^{\theta} &= m\vec{a}_1 + n\vec{a}_2, \\ \vec{Q}^{\bar{\theta}} &= (n+m)\vec{a}_1 - m\vec{a}_2, \end{aligned} \tag{76}$$

where $0 < \theta < \pi/3$ and $-\pi/6 < \bar{\theta} < 0$ are the two possible twist angles (see Fig. 16). The full set of possible twist angles for commensurate structures is determined by

$$\begin{aligned} \cos(\theta) &= \frac{\vec{P}\cdot\vec{Q}^{\theta}}{|\vec{P}||\vec{Q}^{\theta}|} = \frac{3m^2 + 3mr + \frac{1}{2}r^2}{3m^2 + 3mr + r^2}, \\ \cos(\bar{\theta}) &= \frac{\vec{P}\cdot\vec{Q}^{\bar{\theta}}}{|\vec{P}||\vec{Q}^{\bar{\theta}}|} = \frac{\frac{3}{2}\bar{m}^2 + 3\bar{m}\bar{r} + \bar{r}^2}{3\bar{m}^2 + 3\bar{m}\bar{r} + \bar{r}^2}, \end{aligned} \tag{77}$$

where we have defined $r = n - m$ and the bar notation indicates the correspondence to the twist angle. The $\vec{Q}$ points can then be rewritten as

$$\begin{aligned} \vec{Q}^{\theta}(m, r) &= m\vec{a}_1 + (m+r)\vec{a}_2, \\ \vec{Q}^{\bar{\theta}}(\bar{m}, \bar{r}) &= (\bar{r} + 2\bar{m})\vec{a}_1 - \bar{m}\vec{a}_2. \end{aligned} \tag{78}$$

The primitive translation vectors for twist angle θ are determined by the minimal m and r that satisfy Eq. (77) (a similar argument can be given for $\bar{\theta}$). If $\gcd(m, r) \neq 1$, then m and r can be reduced by dividing out their common factors. If $\gcd(m, r) = 1$, then we are left with two cases. Suppose $\gcd(r, 3) = 1$, then m and r are minimized, so one primitive translation vector is given by $\vec{A}_1 = \vec{Q}^{\theta}(m, r) = m\vec{a}_1 + (m+r)\vec{a}_2$ (a second one can be found by rotation of $\vec{A}_1$ by $\pi/3$). If $\gcd(r, 3) = 3$, then we can write

$$\frac{3m^2 + 3mr + \frac{1}{2}r^2}{3m^2 + 3mr + r^2} = \frac{m^2 + 3mr' + \frac{1}{2}3(r')^2}{m^2 + 3mr' + 3(r')^2}, \tag{79}$$

with $r = 3r'$, and we recognize the second expression in Eq. (77) with $\bar{m} \mapsto r'$ and $\bar{r} \mapsto m$. This leads to the primitive vector $\vec{A}_1 = R(\vec{Q}^{\bar{\theta}}(r', m)) = (m + r/3)\vec{a}_1 + r/3\vec{a}_2$, where $R(\vec{Q})$ represents a reflection of $\vec{Q}$ along the symmetry axis between $\vec{P}$ and $\vec{Q}$ (see Fig. 16). The other primitive vector can again be found by rotating the result by $\pi/3$. Assuming $\gcd(m, r) = 1$, the primitive vectors for the Moiré superlattice are thus given by:

If $\gcd(r, 3) = 1$,

$$\begin{pmatrix} \vec{A}_1 \\ \vec{A}_2 \end{pmatrix} = \begin{pmatrix} m & m+r \\ -(m+r) & 2m+r \end{pmatrix} \begin{pmatrix} \vec{a}_1 \\ \vec{a}_2 \end{pmatrix}. \tag{80}$$

If $\gcd(r, 3) = 3$,

$$\begin{pmatrix} \vec{A}_1 \\ \vec{A}_2 \end{pmatrix} = \begin{pmatrix} m + \frac{1}{3}r & \frac{1}{3}r \\ -\frac{1}{3}r & m + \frac{2}{3}r \end{pmatrix} \begin{pmatrix} \vec{a}_1 \\ \vec{a}_2 \end{pmatrix}. \tag{81}$$

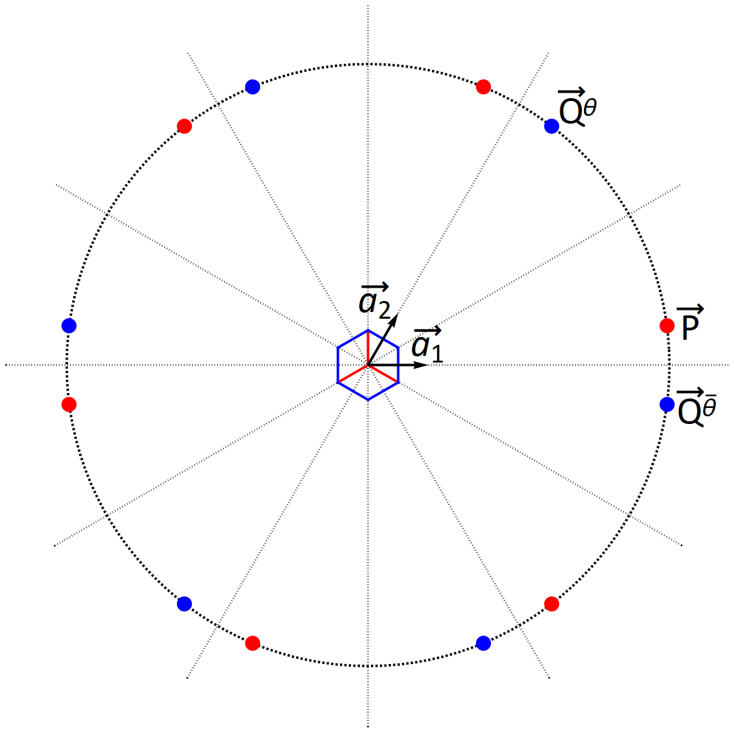

Figure 16: $\vec{P}$ and $\vec{Q}$ points on a shell centered on the rotation center. In the middle of the picture, a piece of an $A-B$ stacked layer is shown with lattice vectors $\vec{a}_1$ and $\vec{a}_2$. The symmetry of the lattice implies that the $\vec{P}$ and $\vec{Q}$ points come in pairs of six. Commensurate structures can be obtained by rotating the $\vec{P}$ point indicated in the figure to the $\vec{Q}^{\theta}$ or $\vec{Q}^{\bar{\theta}}$ point.

The reciprocal lattice vectors of the Moiré pattern are then given by

$$\begin{pmatrix}\vec{G}_1\\ \vec{G}_2\end{pmatrix} = \frac{4\pi}{3|\vec{A}_1|}\begin{pmatrix}2 & -1\\ -1 & 2\end{pmatrix}\begin{pmatrix}\vec{A}_1\\ \vec{A}_2\end{pmatrix}. \tag{82}$$

The Dirac points of the unrotated and rotated layer are given by $\vec{K} = (4\pi/3)(\vec{a}_1 - \vec{a}_2)$ and $\vec{K}^{\theta} = (4\pi/3)(\vec{a}'_1 - \vec{a}'_2)$ respectively. According to Ref. [76], "after some tedious but trivial algebra", it can be found that

$$\Delta\vec{K} := \vec{K}^{\theta} - \vec{K} = \begin{cases} \frac{r}{3}(2\vec{G}_1 + \vec{G}_2) & \text{if } \gcd(r,3) = 1, \\ \frac{r}{3}(\vec{G}_1 + \vec{G}_2) & \text{if } \gcd(r,3) = 3. \end{cases} \tag{83}$$

4.2 Hamiltonian of twisted bilayer graphene

This section is based on Refs. [76] and [29]. Recall from Section 2.3 that for single-layer graphene, the tight-binding Hamiltonian is given by

$$\mathcal{H} = \sum_{l,l',\langle\langle\vec{r},\vec{r}'\rangle\rangle,\sigma} c^\dagger_{l,\vec{r},\sigma} c_{l',\vec{r}',\sigma} \langle l,\vec{r},\sigma|\mathcal{H}|l',\vec{r}',\sigma\rangle. \tag{84}$$

In the continuum limit, we can replace the particle operators $c^\dagger$ and $, c$ by field operators $\psi^\dagger$ and ψ that vary slowly on the scale of a graphene unit cell, because the Moiré superlattice unit cells become very large for small twist angles. The corresponding transformation for the first (unrotated) layer can be given by $c_\alpha(\vec{r}) \to v_c^{1/2}\psi_{1,\alpha}(\vec{r})e^{i\vec{K}\cdot\vec{r}}$. As mentioned in Section 2.3, the dispersion can be described by the Dirac Hamiltonian in the vicinity of a K-point. This leads to the single-layer Hamiltonians

$$\begin{aligned}
\mathcal{H}_1 &= v_c \sum_{l,\sigma,\vec{k}} \psi^\dagger_{1,l,\vec{k},\sigma}\psi_{1,l,\vec{k},\sigma}(\epsilon_0 - 3t')\mathbb{1} + \hbar v_c \sum_{\substack{l\neq l'\\ \sigma,\vec{k}}} \psi^\dagger_{1,l,\vec{k},\sigma}\psi_{1,l',\vec{k},\sigma} v_F(\tau\cdot\vec{k}),\\
\mathcal{H}_2 &= v_c \sum_{l,\sigma,\vec{k}} \psi^\dagger_{2,l,\vec{k},\sigma}\psi_{2,l,\vec{k},\sigma}(\epsilon_0 - 3t')\mathbb{1}^\theta + \hbar v_c \sum_{\substack{l\neq l'\\ \sigma,\vec{k}}} \psi^\dagger_{1,l,\vec{k},\sigma}\psi_{1,l',\vec{k},\sigma} v_F(\tau^\theta\cdot\vec{k}),
\end{aligned} \tag{85}$$

where the subscripts 1 and 2 denote the first (unrotated) and second (rotated) layer, respectively, $\mathbb{1}^\theta = e^{i\theta\tau_z/2}\mathbb{1}e^{-i\theta\tau_z/2}$, and $\tau = \begin{pmatrix}\tau_x & \tau_y\end{pmatrix}$, $\tau^\theta = e^{i\theta\tau_z/2}\tau e^{-i\theta\tau_z/2}$ with τ_x, τ_y, τ_z Pauli matrices. For the inter-layer Hamiltonian, we define the parameter $\vec{\delta}(\vec{r})$ that represents the horizontal (in-plane) distance between a site $\vec{r}$ in layer m and sublattice l to its nearest neighbor in layer $m' \neq m$, residing in sublattice l'. This gives rise to

$$\mathcal{H}_\perp = \sum_{\substack{m\neq m'\\ l,l',\vec{r},\sigma}} t_\perp(\vec{r}) c^\dagger_{m,l,\vec{r},\sigma} c_{m',l',\vec{r}+\vec{\delta}(\vec{r}),\sigma}, \tag{86}$$

where $t_\perp(\vec{r}) \equiv t_\perp(\vec{\delta}(\vec{r}))$ describes the inter-layer hopping. If we take the continuum limit of this Hamiltonian and write $\psi_{2,l',\vec{r}+\vec{\delta}(\vec{r}),\sigma} \approx \psi_{2,l',\vec{r},\sigma}$ (because ψ is a slowly varying field), and then take the Fourier transform, we will be led to

$$\mathcal{H}_\perp = v_c \sum_{l,l',\vec{k},\vec{k}',\vec{G},\sigma} \Big(\tilde{t}_\perp(\vec{G})\psi^\dagger_{1,l,\vec{k}+\frac{1}{2}\Delta\vec{K}+\vec{G},\sigma}\psi_{2,l',\vec{k}'-\frac{1}{2}\Delta\vec{K},\sigma}\delta_{(\vec{k}+\frac{1}{2}\Delta\vec{K})(\vec{k}'-\frac{1}{2}\Delta\vec{K})} + h.c.\Big), \tag{87}$$

where $\vec{G}$ is a reciprocal lattice vector and

$$\tilde{t}_\perp(\vec{G}) = \int \mathrm{d}\vec{r}\, t_\perp(\vec{r}) e^{-i\vec{G}\cdot\vec{r}} e^{i\vec{K}^\theta\cdot\vec{\delta}(\vec{r})}. \tag{88}$$

If we assume a commensurate structure with $\gcd(r,3) = 3$ (the meaning of r is defined in Section 4.1), then $\Delta\vec{K}$ will be a reciprocal lattice vector, such that we can write

$$\mathcal{H}_\perp = v_c \sum_{l,l',\vec{k},\vec{G},\sigma} \Big(\tilde{t}_\perp(\vec{G})\psi^\dagger_{1,l,\vec{k}+\frac{1}{2}\Delta\vec{K}+\vec{G},\sigma}\psi_{2,l',\vec{k}-\frac{1}{2}\Delta\vec{K},\sigma} + h.c.\Big). \tag{89}$$

Writing $\phi_{m,l,\vec{k},\sigma} = \psi_{m,l,\vec{k}\pm\frac{1}{2}\Delta\vec{K},\sigma}$ with the positive sign for $m = 1$ and the negative sign for $m = 2$, we find the total Hamiltonian

$$\begin{aligned}\mathcal{H}_{tBLG} &= \mathcal{H}_1 + \mathcal{H}_2 + \mathcal{H}_\perp = \\ &= v_c \sum_{l,\sigma,\vec{k}} \phi^\dagger_{1,l,\vec{k},\sigma}\phi_{1,l,\vec{k},\sigma}(\epsilon_0 - 3t')\mathbb{1} + \hbar v_c \sum_{\substack{l\neq l'\\ \sigma,\vec{k}}} \phi^\dagger_{1,l,\vec{k},\sigma}\phi_{1,l',\vec{k},\sigma} v_F \left[\tau\cdot\left(\vec{k}+\frac{1}{2}\Delta\vec{K}\right)\right] + \\ &+ v_c \sum_{l,\sigma,\vec{k}} \phi^\dagger_{2,l,\vec{k},\sigma}\phi_{2,l,\vec{k},\sigma}(\epsilon_0 - 3t')\mathbb{1}^\theta + \hbar v_c \sum_{\substack{l\neq l'\\ \sigma,\vec{k}}} \phi^\dagger_{2,l,\vec{k},\sigma}\phi_{2,l',\vec{k},\sigma} v_F \left[\tau^\theta\cdot\left(\vec{k}-\frac{1}{2}\Delta\vec{K})\right)\right] + \\ &+ v_c \sum_{l,l',\vec{k},\vec{G},\sigma} \left(\tilde{t}_\perp(\vec{G})\phi^\dagger_{1,l,\vec{k}+\vec{G},\sigma}\phi_{2,l',\vec{k},\sigma} + h.c.\right).\end{aligned} \tag{90}$$

The inter-layer hopping parameter $\tilde{t}_\perp(\vec{G})$ has different values, depending on between which sublattices the hopping takes place (see Ref. [28]). The Hamiltonian leads to the dispersion relation that can be seen in Fig. 17. For very small twist angles, the Moiré bands show a quadratic dispersion around the reciprocal lattice points that are denoted by A and B in Fig. 17. This behavior is expected because for a very small twist, the dispersion should be similar to that of an $A-B$ stacked bilayer, which we have seen in Fig. 5 of Section 2.4 to be quadratic around a K-point. For larger twist angles, the sheets decouple, and we are left with a linear dispersion, as we would expect from single-layer graphene. For intermediate angles, the dispersion near the A- and B-points becomes flat. Flat bands typically indicate interesting behavior because since the velocity of the electrons is related to the slope of the dispersion, their kinetic energy becomes zero. This means that the interaction energies will become very important, which may give rise to strongly correlated states, such as superconductivity.

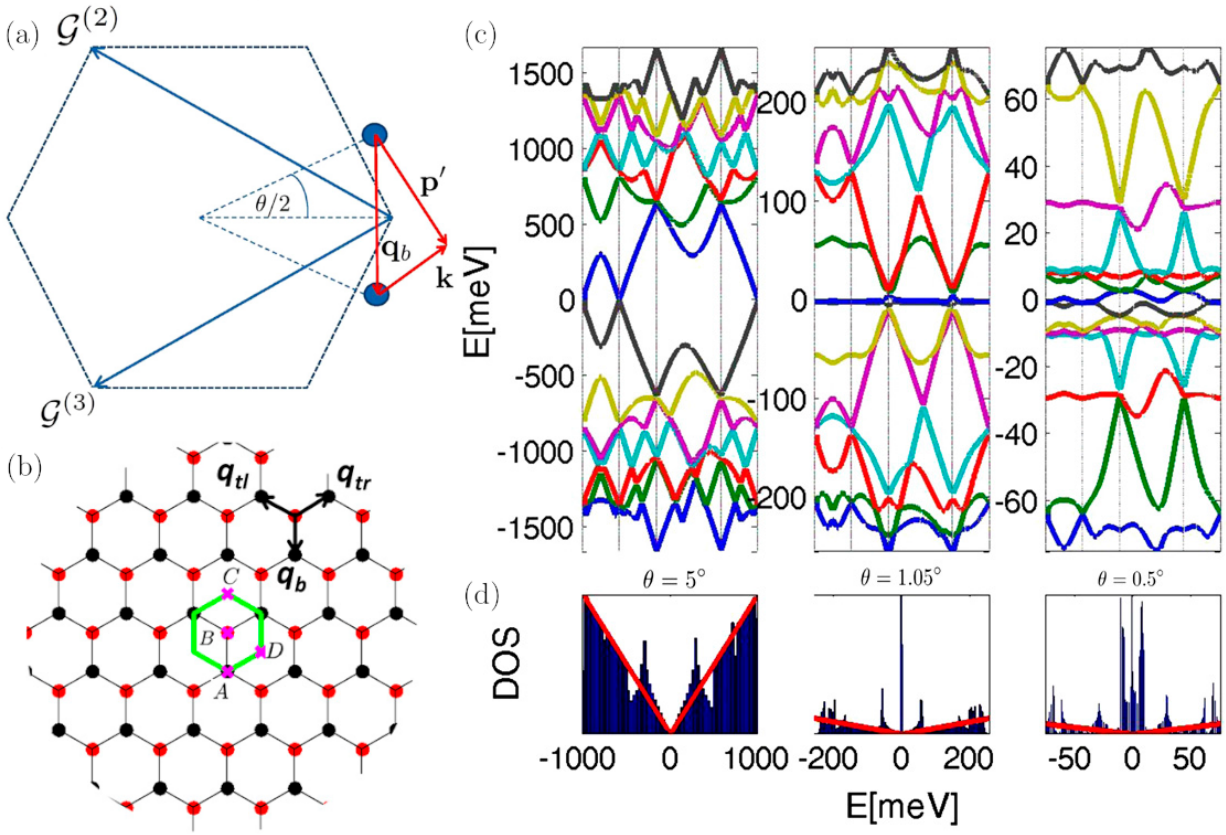

Figure 17: (a) The dashed hexagon denotes the first Brillouin zone of graphene. The blue disks represent the shifted Dirac points of the two layers in tBLG. (b) Reciprocal lattice of the Moiré pattern. (c) Band stucture along the path $A - B - C - D - A$ [see panel (b)] for $\theta = 5°, 1.05°$ and $0.5°$. (d) Density of states. For $\theta = 1.05°$, a van Hove singularity can be seen at zero energy. Figure adapted from Ref. [28]. Here, $(\epsilon_0 - 3t')$ has been set to zero.

4.3 Comparison to high-T_c cuprates

As mentioned in the general introduction, high-T_c cuprates are the superconductors with the highest critical temperature that we currently know of. Unfortunately, it is not yet completely understood how superconductivity takes place in these materials. A picture of the unit cells of some high-T_c cuprates can be seen in Fig. 18. It is known that the superconductivity originates from the $\mathrm{Cu}-\mathrm{O}$ planes [77], yet it is still unclear from where the effective attractive interaction that leads to the formation of Cooper pairs originates [78].

In Section 3.3, we have seen that an effective attractive electron-electron interaction can be derived from the electron-phonon coupling. However, in high-T_c cuprates, the electron-phonon coupling is not likely to be the driving mechanism for superconductivity, because $k_B T_c$ is much larger than the energy scale of the electron-phonon coupling. In addition, small or no isotope effect was observed in $T_c(x)$, where x is the doping concentration. Potentially, the magnetic properties of the cuprates play a role. In the phase diagram of high-T_c cuprates (see Fig. 19), we can see a Mott insulating phase at zero doping. This antiferromagnetic phase is attributed to the highly localized d-orbitals of the copper atoms. These orbitals have a narrow energy band width. This means that these bands will be more flat, implying that the kinetic energy becomes small and the interactions become important there. The Mott insulating phase can be described by the Hubbard model when it is mapped into the antiferromagnetic Heisenberg model [3]. If the material is doped, we will encounter a superconducting phase.

A Mott insulating phase can also be seen in the phase diagram of tBLG (Fig. 19), and when increasing or decreasing the charge carrier density, one will equally find superconducting states. However, in tBLG we only have carbon atoms, which are far less magnetic than copper atoms. This opens the question whether the magnetic properties are related to the superconducting phase of high-T_c cuprates, or whether there are some other contributions that give rise to it. In fact, high-T_c cuprates display a whole zoo of phenomena, and it is not known if and how they are related to superconductivity. Some examples of these phenomena are charge density waves, pseudogap phases, spin glass phases, stripes and spin density waves [79].

The complex structure of high-T_c cuprates (Fig. 18) explains why doping the material is unfavorable when doing experimental research because to investigate the entire phase diagram, one needs to prepare one sample for each doping value. A perk of twisted bilayer graphene is that the charge carrier density can be tuned via a gate-voltage, eliminating the need of chemical doping. TBLG is also much easier to understand theoretically because it is a purely carbon-based material. The critical temperature for the tBLG in Fig. 19 is about 0.3 K, which is very high compared to the charge carrier density. This indicates that tBLG really is a strongly correlated material, making it closely related to high-T_c cuprates. Finally, the properties of tBLG vary vastly depending on the twist angle. This possibly provides a platform to understand the superconductivity mechanism that takes place in high-T_c cuprates, explaining the extensive research done on these systems.

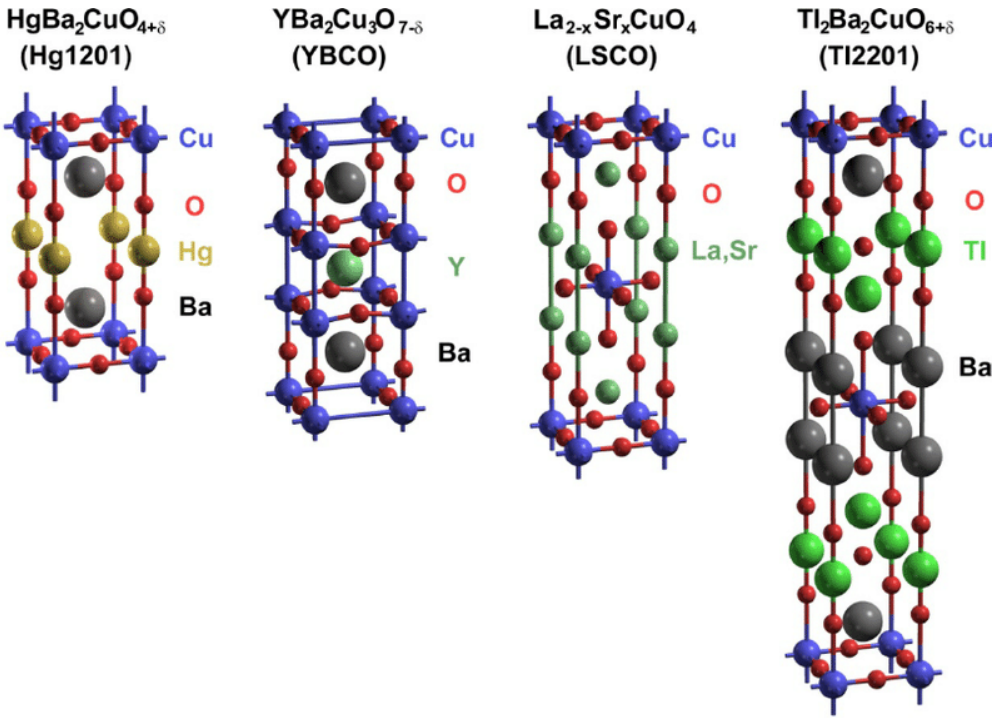

Figure 18: Unit cells of high-T_c cuprates. Figure adapted from Ref. [80].

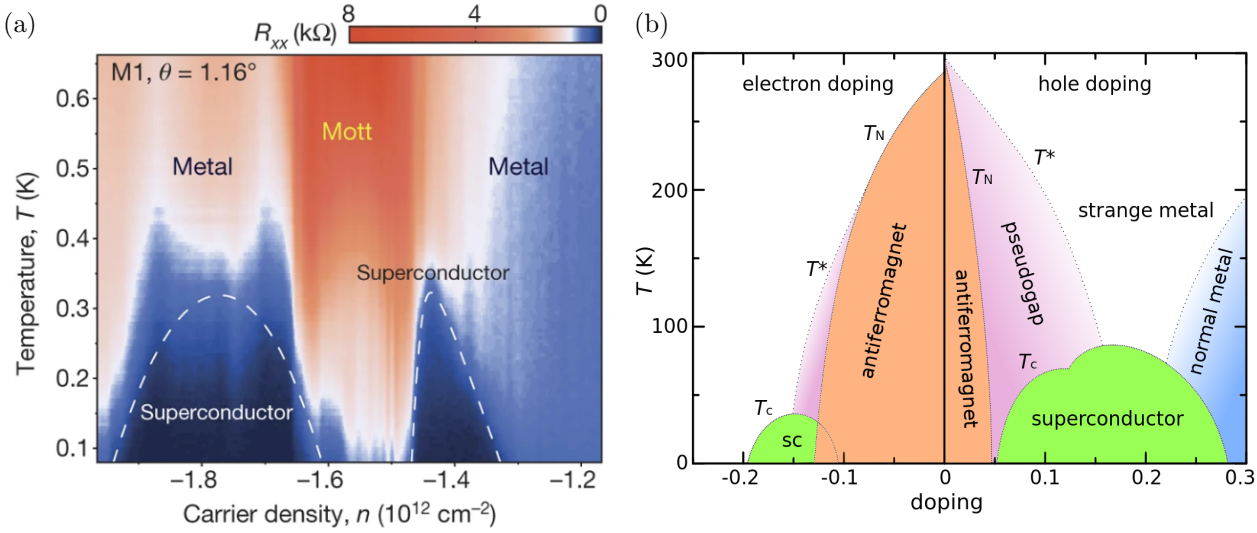

Figure 19: (a) Phase diagram of tBLG with a twist angle of 1.16°. Panel from Ref. [27]. (b) Typical phase diagram of high-T_c cuprates. Panel from Ref. [81].

5 Conclusion

In this thesis, we have studied superconductivity in the context of twisted bilayer graphene, and we have addressed the electronic properties of graphene and its (twisted) bilayer. We have discussed the importance of room-temperature superconductors on the basis of multiple useful applications. As of today, the materials with the highest critical temperature for superconductivity are high-T_c cuprates. Unfortunately, it is not yet understood what is the underlaying mechanism that is responsible for superconductivity because the complicated chemical structure of high-T_c cuprates gives rise to a whole zoo of phenomena, of which it is still unclear if and how they are related to superconductivity. Experimental research on high-T_c cuprates also faces a difficulty, because exploring their phase diagram requires doping, which requires the preparation of a large number of samples. It has been discovered that the phase diagram of twisted bilayer graphene shares similarities with the phase diagram of high-T_c cuprates. Twisted bilayer graphene is purely carbon based, which makes it easier to treat theoretically. Moreover, its phase diagram can be explored by tuning a gate voltage, eliminating the need of chemical doping. This possibly provides a platform to understand the superconductivity mechanism that takes place in high-T_c cuprates.

We have reviewed the electronic properties of graphene using second quantization and have seen that its dispersion can be described by a Dirac Hamiltonian in the vicinity of a K-point. The dispersion relations of bilayer graphene have also been presented, and a van Hove singularity was observed near the M-point. Such a singularity may lead to strongly correlated states because the kinetic energy goes to zero, revealing the effect of interactions, which are amplified due to the diverging density of states. However, the flat band region was too far above the Fermi level. This problem can be solved for magic-angle tBLG. Using the commensurability of the Moiré superstructure that appears in tBLG for certain twist angles, we have constructed a tight-binding Hamiltonian that describes its band structure in the continuum limit. In doing so, a Dirac Hamiltonian was assumed for the intra-layer hopping. For twist angles of approximately $1.1°$, we have seen a flat band at the Fermi level.

The phenomenon of superconductivity was revised, from the macro- and microscopic perspective. A macroscopic approach has been given using the Ginzburg-Landau model, and we have reviewed the Meissner effect that followed from the London equation. A microscopic approach of superconductivity has been discussed following BCS theory, where we assumed an effective attractive electron-electron interaction that arose from the electron-phonon coupling. We have performed a mean-field approximation and have studied the Bogoliubov transformation, which gave rise to the gap equation. Assuming a generic dispersion $E \sim k^\alpha$ and dimensionality d, this last expression allows us to describe superconductivity for systems with non-integer α and d. To the best of our knowledge, it is the first time that such calculations have been performed.

Both in high-T_c cuprates and tBLG, the electron-phonon interaction is not enough to give a complete picture of their phase diagrams. For example, both materials have a Mott insulating ground phase that originates from a repulsive interaction, which is often described by the Hubbard model. It is important to include these interactions in order to get a more clear

view of the entire phase diagram. Next to including more interactions, we could also have considered more complicated pairing symmetries, that are important in cuprates and could be relevant in tBLG. Another element that could be addressed is how one can obtain the Ginzburg-Landau formalism from the BCS theory, connecting the micro- and macroscopic description for superconducting materials. By adding other competing phases, we could then have a more clear view of the phase diagram.

Similarly to high-T_c cuprates, the superconductivity in tBLG is not yet completely understood. However, research on tBLG is much more accessible than in high-T_c cuprates, so hopefully, tBLG will teach us more about the superconductivity phenomenon, such that we can understand the superconductivity in high-T_c cuprates better and eventually come one step closer towards room-temperature superconductivity.

A Reciprocal space

This section is partly based on Ref. [82]. Let $\psi(\vec{x})$ be a wavefunction and define the translation operator $T_{\vec{R}}$ that translates $\vec{x}$ by a lattice vector $\vec{R}$. Note that $T_{\vec{R}}$ commutes with the (periodic) Hamiltonian H because $T_{\vec{R}}H(\vec{x})\psi(\vec{x}) = H(\vec{x}+\vec{R})\psi(\vec{x}+\vec{R}) = H(\vec{x})\psi(\vec{x}+\vec{R}) = H(\vec{x})T_{\vec{R}}\psi(\vec{x})$. This means that $T_{\vec{R}}$ and H have the same eigenstates, so $T_{\vec{R}}\psi(\vec{x}) = C(\vec{R})\psi(\vec{x})$. Translating by $\vec{R}$ and then by $\vec{R}'$ or translating by $\vec{R}+\vec{R}'$ should give the same result, so $T_{\vec{R}'}T_{\vec{R}}\psi(\vec{x}) = T_{\vec{R}+\vec{R}'}\psi(\vec{x})$, which leads to $C(\vec{R})C(\vec{R}')\psi(\vec{x}) = C(\vec{R}+\vec{R}')\psi(\vec{x})$, such that $C(\vec{R})C(\vec{R}') = C(\vec{R}+\vec{R}')$. Then $C(\vec{R})$ is of the form $e^{i\vec{k}\cdot\vec{R}}$ for some $\vec{k}$, which we will refer to as the wavevector from now on. We can now write that

$$\psi_{\vec{k}}(\vec{x}+\vec{R}) = e^{i\vec{k}\cdot\vec{R}}\psi_{\vec{k}}(\vec{x}), \tag{91}$$

and we can see that the periodicity of the lattice is indeed respected, because $|\psi_{\vec{k}}(\vec{x}+\vec{R})|^2 = |e^{i\vec{k}\cdot\vec{R}}\psi_{\vec{k}}(\vec{x})|^2 = |\psi_{\vec{k}}(\vec{x})|^2$.

A more common description of the wavefunction can be found by multiplying Eq. (91) by $e^{-i\vec{k}\cdot(\vec{x}+\vec{R})}$, which leads to $e^{-i\vec{k}\cdot(\vec{x}+\vec{R})}\psi_{\vec{k}}(\vec{x}+\vec{R}) = e^{-i\vec{k}\cdot\vec{x}}\psi_{\vec{k}}(\vec{x})$. Now, write $u(\vec{x}) = e^{-i\vec{k}\cdot\vec{x}}\psi_{\vec{k}}(\vec{x})$. Then $u(\vec{x}+\vec{R}) = u(\vec{x})$, and we can conclude that $\psi_{\vec{k}}(\vec{x}) = e^{i\vec{k}\cdot\vec{x}}u(\vec{x})$ with u a periodic function with the lattice periodicity. This is also known as Bloch's theorem. The wavevector is linked to the momentum by the de Broglie relation $\vec{p} = \hbar\vec{k}$.

Consider a wave $\psi_{\vec{k}}(\vec{x}) = e^{i\vec{k}\cdot\vec{x}}u(\vec{x})$ and let $\vec{R}$ be a lattice vector. There exist wavevectors $\vec{K}$ that yield plane waves with the same periodicity as the lattice. For these $\vec{K}$ one can write $\psi_{\vec{K}}(\vec{x}) = \psi_{\vec{K}}(\vec{x}+\vec{R})$, so $e^{i\vec{K}\cdot\vec{x}}u(\vec{x}) = e^{i\vec{K}\cdot(\vec{x}+\vec{R})}u(\vec{x}+\vec{R}) = e^{i\vec{K}\cdot(\vec{x}+\vec{R})}u(\vec{x})$, such that $e^{i\vec{K}\cdot\vec{R}} = 1$. This condition is fulfilled when $\vec{K}\cdot\vec{R} = 2\pi n$ with $n \in \mathbb{Z}$. The vectors $\vec{K}$ for which this holds, are the reciprocal lattice vectors.

To show that the set of these $\vec{K}$ indeed forms a lattice, notice that it is closed under addition and substraction. This is true because if $\vec{K}, \vec{K}'$ are reciprocal lattice vectors, then $e^{(\vec{K}+\vec{K}')\cdot\vec{R}} = e^{\vec{K}\cdot\vec{R}}e^{\vec{K}'\cdot\vec{R}} = 1\cdot 1 = 1$ and $e^{(\vec{K}-\vec{K}')\cdot\vec{R}} = e^{\vec{K}\cdot\vec{R}}/e^{\vec{K}'\cdot\vec{R}} = 1/1 = 1$, so then $\vec{K}+\vec{K}'$ and $\vec{K}-\vec{K}'$ are also reciprocal lattice vectors. To determine its primitive vectors, construct vectors $\vec{b}_1, \vec{b}_2$ as

$$\begin{aligned} b_1 &= \frac{2\pi}{\Delta} f(\vec{a}_2), \\ b_2 &= -\frac{2\pi}{\Delta} f(\vec{a}_1), \end{aligned} \tag{92}$$

where $f(\vec{a}_i) = f\left(\begin{pmatrix} a_{i.1} & a_{i.2} \end{pmatrix}^T\right) = \begin{pmatrix} a_{i.2} & -a_{i.1} \end{pmatrix}^T$ and $\Delta = \vec{a}_1 \cdot f(\vec{a}_2)$. Notice that with this definition we have $\vec{a}_i \cdot \vec{b}_j = 2\pi\delta_{ij}$. Denote any generic reciprocal lattice vector by $\vec{K} = m_1\vec{b}_1 + m_2\vec{b}_2$ with $m_1, m_2 \in \mathbb{R}$. Assuming that $\vec{K}$ and $\vec{R}$ are reciprocal and direct lattice vectors respectively, we can write that $e^{\vec{K}\cdot\vec{R}} = e^{(m_1\vec{b}_1+m_2\vec{b}_2)\cdot(n_1\vec{a}_1+n_2\vec{a}_2)} = e^{2\pi(m_1n_1+m_2n_2)} = 1$, which can only be true if m_1, m_2 are integers, hence $\vec{b}_1, \vec{b}_2$ are primitive vectors.

Notice that if two wavevectors $\vec{k}'$ and $\vec{k}$ are separated by a reciprocal lattice vector (such that $\vec{k}' = \vec{k} + \vec{K}$), then $\psi_{\vec{k}'}(\vec{R}) = e^{\vec{k}'\cdot\vec{R}}u(\vec{R}) = e^{(\vec{k}+\vec{K})\cdot\vec{R}}u(\vec{R}) = e^{\vec{k}\cdot\vec{R}}e^{\vec{K}\cdot\vec{R}}u(\vec{R}) = e^{\vec{k}\cdot\vec{R}}u(\vec{R}) = \psi_{\vec{k}}(\vec{R})$, so there is essentially no difference between plane waves that originate from wavevectors that differ by a reciprocal lattice vector. In this way, one defines the first Brillouin zone (see Fig. 2), containing the wavevectors that are unique upon translation by reciprocal lattice vectors.

B Second quantization

This section is based on Chapter 21 of Ref. [83]. In first quantization, one represents a state by stating the quantum numbers for every particle in the system. In second quantization, states are represented by the amount of particles that have a certain combination of quantum numbers. In bra-ket notation, we can write this as $|n_1, n_2, \cdots\rangle$, describing a state where n_i particles have quantum numbers $K_i \in K$ where the set K of quantum numbers can describe the entire system (so K is complete). This kind of state lives in Fock space, where any pair of states is orthonormal.

One can transform a state to have an extra particle with quantum numbers K_i by applying the creation operator $c_i^\dagger$. A particle can be removed by applying the annihilation operator c_i. We can now write that

$$\begin{aligned} c_i^\dagger |n_1, n_2, \cdots, n_i, \cdots\rangle &\propto |n_1, n_2, \cdots, n_i + 1, \cdots\rangle , \\ c_i |n_1, n_2, \cdots, n_i, \cdots\rangle &\propto |n_1, n_2, \cdots, n_i - 1, \cdots\rangle . \end{aligned} \tag{93}$$

We must require that the annihilation operator can only work when there actually is a particle to remove, so if a_i would be applied to a state where $n_i = 0$, then $c_i |n_1, n_2, \cdots, n_i, \cdots\rangle = 0$. We will also require that

$$\begin{aligned} c_i^\dagger |\mathbf{0}\rangle = \Psi_i^1 &= |0, 0, \cdots, n_i = 1, \cdots\rangle , \\ c_i \Psi_j^1 = c_i |0, 0, \cdots, n_j = 1, \cdots\rangle &= \delta_{ij} |\mathbf{0}\rangle . \end{aligned} \tag{94}$$

Now, let L be another complete set of quantum numbers. The transformation between the two representations is then given by $|K_i\rangle = \sum_p |L_p\rangle \langle L_p|K_i\rangle$. Then, with creation and annihilation operators $b_p^\dagger$ and b_p that correspond to L,

$$\begin{aligned} c_i^\dagger &= \sum_p b_p^\dagger \langle L_p|K_i\rangle , \\ c_i &= \sum_p \langle K_i|L_p\rangle b_p. \end{aligned} \tag{95}$$

These expressions are consistent with Eq. (94) because

$$\begin{aligned}
\sum_p b_p^\dagger \langle L_p|K_i\rangle |\mathbf{0}\rangle &= \sum_p |L_p\rangle \langle L_p|K_i\rangle = |K_i\rangle = c_i^\dagger |\mathbf{0}\rangle ,\\
\sum_p \langle K_i|L_p\rangle b_p \Psi_j^1 &= \sum_p \langle K_i|L_p\rangle b_p \sum_q \langle L_q|K_j\rangle \Phi_q^1 = \\
&= \sum_{p,q} \langle K_i|L_p\rangle \langle L_q|K_j\rangle b_p \Phi_q^1 = \\
&= \sum_{p,q} \langle K_i|L_p\rangle \langle L_q|K_j\rangle \delta_{pq} |\mathbf{0}\rangle = \\
&= \sum_p \langle K_i|L_p\rangle \langle L_p|K_j\rangle |\mathbf{0}\rangle = \\
&= \delta_{ij} |\mathbf{0}\rangle = c_i \Psi_j^1.
\end{aligned} \tag{96}$$

Note that applying $c_i^\dagger c_j^\dagger$ on a state should give the same result as applying $c_j^\dagger c_i^\dagger$ up to a normalisation factor λ, so we can write $c_i^\dagger c_j^\dagger \Psi = \lambda c_j^\dagger c_i^\dagger \Psi$ where Ψ is a short hand notation for a state. Then

$$(c_i^\dagger c_j^\dagger - \lambda c_j^\dagger c_i^\dagger)\Psi = \sum_{p,q} \langle L_p|K_i\rangle \langle L_q|K_j\rangle \left(b_p^\dagger b_q^\dagger - \lambda b_q^\dagger b_p^\dagger\right)\Psi = 0. \tag{97}$$

The tranformation coefficients $\langle L_p|K_i\rangle , \langle L_q|K_j\rangle$ are arbitrary complex numbers, so we must have that $b_p^\dagger b_q^\dagger - \lambda b_q^\dagger b_p^\dagger = 0 \; \forall p, q$; in particular also $b_q^\dagger b_p^\dagger - \lambda b_p^\dagger b_q^\dagger = 0$. Hence we find $\lambda = \pm 1$ and $c_i^\dagger c_j^\dagger \mp c_j^\dagger c_i^\dagger = 0$. Taking the Hermitian conjugate of this leads to $c_i c_j \mp c_j c_i = 0$. From the creation and annihilation operators, we can now deduce two kinds of particles. The ones for which the creation (and annihilation) operators commute, are called bosons. Particles for which these operators anticommute, are called fermions. We will now derive a commutation relation for the combination of these operators. We can write that $c_i c_j^\dagger \Psi = \mu c_j^\dagger c_i \Psi$, such that

$$(c_i c_j^\dagger - \mu c_j^\dagger c_i)\Psi = \sum_{p,q} \langle K_i|L_p\rangle \langle L_q|K_j\rangle \left(b_p b_q^\dagger - \mu b_q^\dagger b_p\right)\Psi = 0. \tag{98}$$

From the spin-statistics theorem, this will lead to the following commutation relations for bosons and fermions:

For bosons:

$$\begin{aligned}
&[c_i^\dagger, c_j^\dagger] = 0,\\
&[c_i, c_j] = 0,\\
&[c_i, c_j^\dagger] = \delta_{ij}.
\end{aligned} \tag{99}$$

For fermions:

$$\begin{aligned}
&\{c_i^\dagger, c_j^\dagger\} = 0,\\
&\{c_i, c_j\} = 0,\\
&\{c_i, c_j^\dagger\} = \delta_{ij}.
\end{aligned} \tag{100}$$

A consequence of this equation is that, for fermions, $c_i^\dagger c_i^\dagger = 0$, meaning that no two fermions can have the same quantum numbers. This is called Pauli's exclusion principle.

We now define the occupation number operators N_i of which the eigenvalues n_i represent the

amount of particles that have quantum numbers K_i. The sum of these operators $N = \sum_i N_i$ must be invariant because the total amount of particles should not change when switching to another set of quantum numbers. Therefore we must write N as a linear combination of other additive invariant operators, of which the only ones are the identity and $\sum_i c_i^\dagger c_i$. One could argue that $\sum_i c_i c_i^\dagger$ is also invariant, but it can be written as a linear combination of the other two by the commutation relation shown in Eq. (99) and Eq. (100). Any other sum of products of $c_i^\dagger$ and c_i will not be invariant, so N_i will be of the form $xc_i^\dagger c_i + y1$. Now, $N_i |\mathbf{0}\rangle$ should be zero, hence $y = 0$. Additionally, $N_i \Psi_i^1$ should return Ψ_i^1, and using Eq. (94) we find that $x = 1$. Hence

$$N_i = c_i^\dagger c_i. \tag{101}$$

We can now write that

$$\begin{aligned} \langle n_1, n_2, \cdots, n_i, \cdots | N_i | n_1, n_2, \cdots, n_i, \cdots \rangle = n_i = \\ = \langle n_1, n_2, \cdots, n_i, \cdots | c_i^\dagger c_i | n_1, n_2, \cdots, n_i, \cdots \rangle , \end{aligned} \tag{102}$$

such that

$$c_i |n_1, n_2, \cdots, n_i, \cdots\rangle = e^{i\alpha} \sqrt{n_i} |n_1, n_2, \cdots, n_i - 1, \cdots\rangle , \tag{103}$$

where α is a real number. For bosons, it follows that $\alpha = 0$. This leads to the following eigenvalues:

$$\begin{aligned} &\text{For bosons:} \\ c |n\rangle &= \sqrt{n} |n-1\rangle , \\ c^\dagger |n\rangle &= \sqrt{n+1} |n+1\rangle . \end{aligned} \tag{104}$$

$$\begin{aligned} &\text{For fermions:} \\ c |0\rangle &= 0, \\ c |1\rangle &= e^{i\alpha} |0\rangle , \\ c^\dagger |0\rangle &= e^{-i\alpha} |1\rangle , \\ c^\dagger |1\rangle &= 0. \end{aligned} \tag{105}$$

Let $\mathcal{H}$ be an operator that measures the value of an additive one-particle quantity H, such as the kinetic energy or the potential energy of a particle in a field. We can express $\mathcal{H}$ as the sum of operators H_i that work on particles that have quantum numbers K_i such that $\mathcal{H} = \sum_i H_i N_i = \sum_i H_i c_i^\dagger c_i$. If we transform the creation and annihilation operators $c_i^\dagger, c_i$ to an arbitrary set via Eq. (95), we get $\mathcal{H} = \sum_{p,q} b_p^\dagger b_q \langle L_p | H | L_q \rangle$, where we have used $\sum_i \langle L_p | K_i \rangle H_i \langle K_i | L_q \rangle = \langle L_p | H | L_q \rangle$.

Let us now assume that $\mathcal{H}$ denotes the Hamiltonian operator, that for now is only composed of additive one-particle quantities. Then $\mathcal{H}$ will be of the form

$$\mathcal{H} = \sum_{i,j} c_i^\dagger c_j \langle K_i | H | K_j \rangle . \tag{106}$$

We can also include additive two-particle quantities, like the Coulomb potential. The operator $\mathcal{V}$ measures the value of an additive two-particle V, such that

$$\begin{aligned}\mathcal{V} &= \frac{1}{2}\sum_{i\neq j} V_{ij}N_iN_j + \frac{1}{2}\sum_i V_iN_i(N_i-1) = \frac{1}{2}\sum_{i,j} V_{ij}(N_iN_j - N_i\delta_{ij}) = \\ &= \frac{1}{2}\sum_{i,j} V_{ij}(c_i^\dagger c_i c_j^\dagger c_j - c_i^\dagger c_i\delta_{ij}) = \frac{1}{2}\sum_{i,j} V_{ij}c_i^\dagger c_j^\dagger c_j c_i = \\ &= \frac{1}{2}\sum_{i,j}\sum_{p,q,r,s} V_{ij}b_p^\dagger b_q^\dagger b_r b_s \langle L_p|K_i\rangle\langle K_i|L_q\rangle\langle L_r|K_j\rangle\langle K_j|L_s\rangle = \\ &= \frac{1}{2}\sum_{i,j}\sum_{p,q,r,s} b_p^\dagger b_q^\dagger b_r b_s \langle L_pL_r|V|L_qL_s\rangle\,.\end{aligned} \tag{107}$$

Including this in our Hamiltionian yields

$$\mathcal{H} = \sum_{i,j} c_i^\dagger c_j \langle K_i|H|K_j\rangle + \sum_{i,j,m,n} c_i^\dagger c_j^\dagger c_m c_n \langle K_iK_j|V|K_mK_n\rangle\,. \tag{108}$$

C Tight-binding calculation for graphene in first quantization

This section is based on Section 3.3 of Ref. [84]. The wavefunction ψ over the entire lattice can be written as a sum over all unit cells contributing two functions ϕ_1 and ϕ_2 describing the two $2p_z$ orbitals of the C atoms, multiplied by a plane wave (this follows from Bloch's theorem). This yields

$$\psi_{\vec{k}}(\vec{r}) = \frac{1}{\sqrt{N}}\sum_{\vec{R}}^{N} e^{i\vec{k}\cdot\vec{R}}\left[c_1\phi_1(\vec{r}-\vec{R}) + c_2\phi_2(\vec{r}-\vec{R})\right]. \tag{109}$$

The dispersion relation is calculated by

$$E(\vec{k}) = \frac{\int \psi_{\vec{k}}(\vec{r})H\psi_{\vec{k}}(\vec{r})\mathrm{d}\vec{r}}{\int \psi_{\vec{k}}(\vec{r})\psi_{\vec{k}}(\vec{r})\mathrm{d}\vec{r}}, \tag{110}$$

where H is the Hamiltonian. When performing this calculation, the hopping integral $\int \phi_i^{\vec{R}}H\phi_j^{\vec{R}'}\mathrm{d}\vec{r}$ will appear, representing the influence of the atomic potential on the electron orbitals. We will simplify this expression by only accounting for the on-site and nearest-neighbor hopping integrals. When $i=j$ and $\vec{R}=\vec{R}'$, the integral represents the on-site energy, so we can write $\int \phi_i^{\vec{R}}H\phi_j^{\vec{R}'}\mathrm{d}\vec{r} = \epsilon_0$. It equals t when the combination of i,j,$\vec{R}$ and $\vec{R}'$ represent nearest neighbors (that is when $i\neq j$ and $\vec{R}$ and $\vec{R}'$ are either equal or separated by $\vec{a}_1$ or $\vec{a}_2$). It is zero elsewhere. The overlap integral $\int \phi_{\vec{k}}(\vec{r})\phi_{\vec{k}}(\vec{r})\mathrm{d}\vec{r}$ is equal to $\delta_{i,j}$ so that the orbitals on

different atoms are assumed to have no influence on each other's shape. In matrix form, the Hamiltonian for this system in momentum space reads

$$\begin{aligned} H = & \begin{array}{c} \\ A \\ B \end{array} \begin{array}{c} \begin{array}{cc} A & B \end{array} \\ \begin{pmatrix} \epsilon_0 & t(1+e^{-i\vec{k}\cdot\vec{a}_1}+e^{-i\vec{k}\cdot\vec{a}_2}) \\ t(1+e^{i\vec{k}\cdot\vec{a}_1}+e^{i\vec{k}\cdot\vec{a}_2}) & \epsilon_0 \end{pmatrix} \end{array} = \\ & = \epsilon_0 \mathbb{1} + d_x(\vec{k})\sigma_x + d_y(\vec{k})\sigma_y, \end{aligned} \tag{111}$$

where

$$\begin{aligned} d_x(\vec{k}) &= t\left[1+\cos(\vec{k}\cdot\vec{a}_1)+\cos(\vec{k}\cdot\vec{a}_2)\right], \\ d_y(\vec{k}) &= t\left[\sin(\vec{k}\cdot\vec{a}_1)+\sin(\vec{k}\cdot\vec{a}_2)\right]. \end{aligned} \tag{112}$$

Using the variational principle, one can now find that

$$\begin{pmatrix} \epsilon_0 - E & t(1+e^{-i\vec{k}\cdot\vec{a}_1}+e^{-i\vec{k}\cdot\vec{a}_2}) \\ t(1+e^{i\vec{k}\cdot\vec{a}_1}+e^{i\vec{k}\cdot\vec{a}_2}) & \epsilon_0 - E \end{pmatrix} \begin{pmatrix} c_1 \\ c_2 \end{pmatrix} = \begin{pmatrix} 0 \\ 0 \end{pmatrix}. \tag{113}$$

Solving this eigenvalue problem yields

$$E_{nn}(\vec{k}) = \epsilon_0 \pm t\gamma(\vec{k}) \tag{114}$$

where

$$\gamma(\vec{k}) = \sqrt{3 + 2\cos(\vec{k}\cdot\vec{a}_1) + 2\cos(\vec{k}\cdot\vec{a}_2) + 2\cos(\vec{k}\cdot(\vec{a}_1-\vec{a}_2))}. \tag{115}$$

It is possible to extend this calculation to include next-nearest neighbors. Denote the value of the hopping integral $\int \phi_i^{\vec{R}} H \phi_j^{\vec{R}'} \mathrm{d}\vec{r}$ by t' for next-nearest neighbors. These occur when $i = j$ and $\vec{R}$ is separated from $\vec{R}'$ by either $\vec{a}_1$, $\vec{a}_2$ or $\vec{a}_2 - \vec{a}_1$ (note that there are now six nearest neighbors). The Hamiltonian for this system is given by

$$\begin{aligned} H = & \begin{array}{c} \\ A \\ B \end{array} \begin{array}{c} \begin{array}{cc} A & B \end{array} \\ \begin{pmatrix} \epsilon_0 + t'\gamma'(\vec{k}) & t(1+e^{-i\vec{k}\cdot\vec{a}_1}+e^{-i\vec{k}\cdot\vec{a}_2}) \\ t(1+e^{i\vec{k}\cdot\vec{a}_1}+e^{i\vec{k}\cdot\vec{a}_2}) & \epsilon_0 + t'\gamma'(\vec{k}) \end{pmatrix} \end{array} = \\ & = d_{\mathbb{1}}(\vec{k})\mathbb{1} + d_x(\vec{k})\sigma_x + d_y(\vec{k})\sigma_y, \end{aligned} \tag{116}$$

where

$$\begin{aligned} d_{\mathbb{1}}(\vec{k}) &= \epsilon_0 + t'\gamma'(\vec{k}), \\ d_x(\vec{k}) &= t\left[1+\cos(\vec{k}\cdot\vec{a}_1)+\cos(\vec{k}\cdot\vec{a}_2)\right], \\ d_y(\vec{k}) &= t\left[\sin(\vec{k}\cdot\vec{a}_1)+\sin(\vec{k}\cdot\vec{a}_2)\right], \end{aligned} \tag{117}$$

and

$$\begin{aligned}\gamma'(\vec{k}) &= e^{i\vec{k}\cdot\vec{a}_1} + e^{i\vec{k}\cdot\vec{a}_2} + e^{i\vec{k}\cdot(\vec{a}_1-\vec{a}_2)} + e^{-i\vec{k}\cdot\vec{a}_1} + e^{-i\vec{k}\cdot\vec{a}_2} + e^{i\vec{k}\cdot(\vec{a}_2-\vec{a}_1)} = \\ &= 2\left[\cos(\vec{k}\cdot\vec{a}_1) + \cos(\vec{k}\cdot\vec{a}_2) + \cos(\vec{k}\cdot(\vec{a}_1-\vec{a}_2))\right].\end{aligned} \tag{118}$$

This results in the following matrix equation:

$$\begin{pmatrix} \epsilon_0 + t'\gamma'(\vec{k}) - E & t(1+e^{-i\vec{k}\cdot\vec{a}_1} + e^{-i\vec{k}\cdot\vec{a}_2}) \\ t(1+e^{i\vec{k}\cdot\vec{a}_1} + e^{i\vec{k}\cdot\vec{a}_2}) & \epsilon_0 + t'\gamma'(\vec{k}) - E \end{pmatrix} \begin{pmatrix} c_1 \\ c_2 \end{pmatrix} = \begin{pmatrix} 0 \\ 0 \end{pmatrix}. \tag{119}$$

The dispersion relation (plotted in Fig. 3) is then given by

$$E_{nnn}(\vec{k}) = \epsilon_0 + t'\gamma'(\vec{k}) \pm t\gamma(\vec{k}). \tag{120}$$

D Bogoliubov transformation

A Bogoliubov tranformation is a linear transformation of creation and annihilation operators that defines new creation and annihilation operators and, as such, redefines the vacuum of the system. Generally, a Bogoliubov tranformation is given by

$$\begin{pmatrix} \gamma_1 \\ \vdots \\ \gamma_n \\ \gamma_1^\dagger \\ \vdots \\ \gamma_n^\dagger \end{pmatrix} = \begin{pmatrix} u_{11} & \dots & u_{1n} & v_{11} & \dots & v_{1n} \\ \vdots & \ddots & \vdots & \vdots & \ddots & \vdots \\ u_{n1} & \dots & u_{nn} & v_{n1} & \dots & v_{nn} \\ v_{11}^* & \dots & v_{1n}^* & u_{11}^* & \dots & u_{1n}^* \\ \vdots & \ddots & \vdots & \vdots & \ddots & \vdots \\ v_{n1}^* & \dots & v_{nn}^* & u_{n1}^* & \dots & u_{nn}^* \end{pmatrix} \begin{pmatrix} c_1 \\ \vdots \\ c_n \\ c_1^\dagger \\ \vdots \\ c_n^\dagger \end{pmatrix}, \tag{121}$$

with $c_j^\dagger, c_j$ particle creation and annihilation operators respectively and $\gamma_i^\dagger, \gamma_i$ the Bogoliubon creation and annihilation operators. The indices i, j represent quantum numbers. In summation notation, the transformation is given by

$$\begin{aligned}\gamma_i &= \sum_j (u_{ij}c_j + v_{ij}c_j^\dagger), \\ \gamma_i^\dagger &= \sum_j (u_{ij}^* c_j^\dagger + v_{ij}^* c_j).\end{aligned} \tag{122}$$

Now assume that the $c_j^\dagger, c_j$ operators create and annihilate electrons, and thus obey the fermionic anticommutation relations. We can make the Bogoliubov operators satisfy the

fermionic anticommutation relations as well by imposing some constraints. Now,

$$\begin{aligned}
\gamma_i\gamma_{i'} + \gamma_{i'}\gamma_i &= \sum_j \sum_{j'} (u_{ij}u_{i'j'}\{c_j c_{j'}\} + u_{ij}v_{i'j'}\{c_j c_{j'}^\dagger\} + v_{ij}u_{i'j'}\{c_j^\dagger c_{j'}\} + v_{ij}v_{i'j'}\{c_j^\dagger c_{j'}^\dagger\}) = \\
&= \sum_j \sum_{j'} (u_{ij}v_{i'j'}\delta_{jj'} + v_{ij}u_{i'j'}\delta_{jj'}) = \\
&= \sum_j (u_{ij}v_{i'j} + v_{ij}u_{i'j}), \\
\gamma_i^\dagger\gamma_{i'} + \gamma_{i'}\gamma_i^\dagger &= \sum_j \sum_{j'} (u_{ij}^* u_{i'j'}\{c_j^\dagger c_{j'}\} + u_{ij}^* v_{i'j'}\{c_j^\dagger c_{j'}^\dagger\} + v_{ij}^* u_{i'j'}\{c_j c_{j'}\} + v_{ij}^* v_{i'j'}\{c_j c_{j'}^\dagger\}) = \\
&= \sum_j \sum_{j'} (u_{ij}^* u_{i'j'}\delta_{jj'} + v_{ij}^* v_{i'j'}\delta_{jj'}) = \\
&= \sum_j (u_{ij}^* u_{i'j} + v_{ij}^* v_{i'j}),
\end{aligned} \tag{123}$$

so if we impose the constraints $\sum_j (u_{ij}v_{i'j} + v_{ij}u_{i'j}) = 0$ and $\sum_j (u_{ij}^* u_{i'j} + v_{ij}^* v_{i'j}) = \delta_{ii'}\ \ \forall i, i'$, the Bogoliubov operators satisfy

$$\begin{aligned}
\{\gamma_i, \gamma_{i'}\} &= 0, \\
\{\gamma_i^\dagger, \gamma_{i'}^\dagger\} &= 0, \\
\{\gamma_i^\dagger, \gamma_{i'}\} &= \delta_{ii'}.
\end{aligned} \tag{124}$$

Now, we will only consider the terms that occur in the BCS Hamiltonian, so

$$\begin{pmatrix} \gamma_{\vec{k},\uparrow} \\ \gamma_{-\vec{k},\downarrow} \\ \gamma_{\vec{k},\uparrow}^\dagger \\ \gamma_{-\vec{k},\downarrow}^\dagger \end{pmatrix} = \begin{pmatrix} u_{11} & u_{12} & v_{11} & v_{12} \\ u_{21} & u_{22} & v_{21} & v_{22} \\ v_{11}^* & v_{12}^* & u_{11}^* & u_{12}^* \\ v_{21}^* & v_{22}^* & u_{21}^* & u_{22}^* \end{pmatrix} \begin{pmatrix} c_{\vec{k},\uparrow} \\ c_{-\vec{k},\downarrow} \\ c_{\vec{k},\uparrow}^\dagger \\ c_{-\vec{k},\downarrow}^\dagger \end{pmatrix}, \tag{125}$$

where the complex parameters u_{ij}, v_{ij} depend on $\vec{k}$. We can set some matrix elements to zero if we associate the Bogobliubov annihilation operator $\gamma_{\vec{k},\uparrow}$ with destroying an electron with quantum numbers $\vec{k},\uparrow$ and creating a hole with quantum numbers $-\vec{k},\downarrow$, and the Bogobliubov creation operator $\gamma_{-\vec{k},\downarrow}^\dagger$ operator with creating an electron with quantum numbers $-\vec{k},\downarrow$ and destroying a hole with quantum numbers $\vec{k},\uparrow$. We can justify this choice by noting that setting one of u_{ij}, v_{ij}^* to zero does not change the fermionic anticommutation relations and it avoids the emergence of terms like $c_{\vec{k},\uparrow}c_{\vec{k},\uparrow}$ which are equal to zero. With this, the matrix equation reduces to

$$\begin{pmatrix} \gamma_{\vec{k},\uparrow} \\ \gamma_{-\vec{k},\downarrow} \\ \gamma_{\vec{k},\uparrow}^\dagger \\ \gamma_{-\vec{k},\downarrow}^\dagger \end{pmatrix} = \begin{pmatrix} u_{11} & 0 & 0 & v_{12} \\ 0 & u_{22} & v_{21} & 0 \\ 0 & v_{12}^* & u_{11}^* & 0 \\ v_{21}^* & 0 & 0 & u_{22}^* \end{pmatrix} \begin{pmatrix} c_{\vec{k},\uparrow} \\ c_{-\vec{k},\downarrow} \\ c_{\vec{k},\uparrow}^\dagger \\ c_{-\vec{k},\downarrow}^\dagger \end{pmatrix}, \tag{126}$$

together with the constraints

$$\begin{aligned} u_{11}v_{21} + v_{12}u_{22} &= 0, \\ |u_{11}|^2 + |v_{12}|^2 &= 1, \\ |v_{21}|^2 + |u_{22}|^2 &= 1. \end{aligned} \tag{127}$$

The Bogoliubov operators are then given by

$$\begin{aligned} \gamma_{\vec{k},\uparrow} &= u_{11}c_{\vec{k},\uparrow} + v_{12}c^\dagger_{-\vec{k},\downarrow}, \\ \gamma^\dagger_{-\vec{k},\downarrow} &= v^*_{21}c_{\vec{k},\uparrow} + u^*_{22}c^\dagger_{-\vec{k},\downarrow}. \end{aligned} \tag{128}$$

Now,

$$\begin{aligned} \frac{1}{v_{12}}\gamma_{\vec{k},\uparrow} - \frac{1}{u^*_{22}}\gamma^\dagger_{-\vec{k},\downarrow} &= \Big(\frac{u_{11}}{v_{12}} - \frac{v^*_{21}}{u^*_{22}}\Big)c_{\vec{k},\uparrow} = \Big(\frac{u_{11}u^*_{22} - v^*_{21}v_{12}}{v_{12}u^*_{22}}\Big)c_{\vec{k},\uparrow}, \\ \frac{1}{u_{11}}\gamma_{\vec{k},\sigma} - \frac{1}{v^*_{21}}\gamma^\dagger_{-\vec{k},\downarrow} &= \Big(\frac{v_{12}}{u_{11}} - \frac{u^*_{22}}{v^*_{21}}\Big)c^\dagger_{-\vec{k},\downarrow} = \Big(\frac{v_{12}v^*_{21} - u^*_{22}u_{11}}{u_{11}v^*_{21}}\Big)c^\dagger_{-\vec{k},\downarrow}, \end{aligned} \tag{129}$$

such that

$$\begin{aligned} c_{\vec{k},\uparrow} &= \frac{u^*_{22}}{u_{11}u^*_{22} - v^*_{21}v_{12}}\gamma_{\vec{k},\uparrow} - \frac{v_{12}}{u_{11}u^*_{22} - v^*_{21}v_{12}}\gamma^\dagger_{-\vec{k},\downarrow} = U^*_{22}\gamma_{\vec{k},\uparrow} - V_{12}\gamma^\dagger_{-\vec{k},\downarrow}, \\ c^\dagger_{-\vec{k},\downarrow} &= \frac{u_{11}}{u_{11}u^*_{22} - v^*_{21}v_{12}}\gamma^\dagger_{-\vec{k},\downarrow} - \frac{v^*_{21}}{u_{11}u^*_{22} - v^*_{21}v_{12}}\gamma_{\vec{k},\uparrow} = U_{11}\gamma^\dagger_{-\vec{k},\downarrow} - V^*_{21}\gamma_{\vec{k},\uparrow}. \end{aligned} \tag{130}$$

From the earlier imposed constraints, it follows that $U_{11}V_{21} + V_{12}U_{22} = 0$ and

$$|U_{22}|^2 + |V_{21}|^2 = |U_{11}|^2 + |V_{12}|^2 = |U_{22}|^2 + |V_{12}|^2 = |U_{11}|^2 + |V_{21}|^2 = 1. \tag{131}$$

This implies that $|U_{22}|^2 = |U_{11}|^2$ and $|V_{12}|^2 = |V_{21}|^2$. Because $U_{11}V_{21} + V_{12}U_{22} = 0$, we can write $V_{\vec{k}} = V_{21} = -V_{12}$ and $U_{\vec{k}} = U_{11} = U_{22}$. This on its turn implies that $u_{\vec{k}} = u_{11} = u_{22}$ and $v_{\vec{k}} = v_{21} = -v_{12}$, such that eventually, $U_{\vec{k}} = u_{\vec{k}}$ and $V_{\vec{k}} = v_{\vec{k}}$. Thus, we can write the Bogoliubov operators as

$$\begin{aligned} \gamma_{\vec{k},\uparrow} &= u_{\vec{k}}c_{\vec{k},\uparrow} - v_{\vec{k}}c^\dagger_{-\vec{k},\downarrow}, \\ \gamma^\dagger_{-\vec{k},\downarrow} &= u^*_{\vec{k}}c^\dagger_{-\vec{k},\uparrow} + v^*_{\vec{k}}c_{\vec{k},\uparrow}, \end{aligned} \tag{132}$$

and the electron annihilation and creation operators as

$$\begin{aligned} c_{\vec{k},\uparrow} &= u^*_{\vec{k}}\gamma_{\vec{k},\uparrow} + v_{\vec{k}}\gamma^\dagger_{-\vec{k},\downarrow}, \\ c^\dagger_{-\vec{k},\downarrow} &= u_{\vec{k}}\gamma^\dagger_{-\vec{k},\downarrow} - v^*_{\vec{k}}\gamma_{\vec{k},\uparrow}. \end{aligned} \tag{133}$$

References

[1] J. F. Annett, *Superconductivity, Superfluids and Condensates*. Great Clarendon Street, Oxford OX2 6DP, United Kingdom: Oxford University Press, 1993.

[2] K. Bennemann and J. Ketterson, *Superconductivity*. Great Clarendon Street, Oxford OX2 6DP, United Kingdom: Oxford University Press, 1993, vol. Volume 1: Conventional and Unconventional Superconductors.

[3] E. C. Marino, *Quantum Field Theory Approach to Condensed Matter Physics*. University Printing House, Cambridge CB2 8BS, United Kingdom: Cambridge University Press, 1993.

[4] H. K. Onnes, "Further experiments with liquid helium. C. on the change of electric resistance of pure metals at very low temperatures etc. IV. the resistance of pure mercury at helium temperatures," *KNAW, Proceedings*, vol. 13 II, pp. 1274–1276, 1911. [Online]. Available: https://www.dwc.knaw.nl/toegangen/digital-library-knaw/?pagetype=publDetail&pId=PU00013358

[5] ——, "Further experiments with liquid helium. D. on the change of electrical resistance of pure metals at very low temperatures, etc. V. the disappearance of the resistance of mercury," *KNAW, Proceedings*, vol. 14 I, pp. 113–115, 1911. [Online]. Available: https://www.dwc.knaw.nl/toegangen/digital-library-knaw/?pagetype=publDetail&pId=PU00013124

[6] G. Katti, S. A. Ara, and A. Shireen, "Magnetic resonance imaging (MRI)–a review," *International journal of dental clinics*, vol. 3, no. 1, pp. 65–70, 2011. [Online]. Available: https://link-gale-com.proxy.library.uu.nl/apps/doc/A346926655/AONE?u=utrecht&sid=AONE&xid=e75b6961

[7] A. Nowogrodzki, "The worlds strongest MRI machines are pushing human imaging to new limits," *Nature*, vol. 563, pp. 24–26, Oct 2018. [Online]. Available: https://spectrum.ieee.org/biomedical/imaging/the-worlds-most-powerful-mri-takes-shape

[8] "Maglev," *Shanghai Airport Authority*, Feb 2015. [Online]. Available: https://web.archive.org/web/20150217050443/http://en.shairport.com:80/2012-11/09/content_15904433.htm

[9] "Japan's maglev train breaks world speed record with 600km/h test run," *The Guardian*, Apr 2015. [Online]. Available: https://www.theguardian.com/world/2015/apr/21/japans-maglev-train-notches-up-new-world-speed-record-in-test-run

[10] Hyung-Woo Lee, Ki-Chan Kim, and Ju Lee, "Review of maglev train technologies," *IEEE Transactions on Magnetics*, vol. 42, no. 7, pp. 1917–1925, 2006. [Online]. Available: https://ieeexplore.ieee.org/abstract/document/1644911

[11] M. Rabinowitz, "Superconducting power generation," *Power Engineering Review, IEEE*, vol. 20, pp. 8 – 11, 06 2000. [Online]. Available: https://ieeexplore.ieee.org/abstract/document/841343

[12] [Online]. Available: https://ecoswing.eu/

[13] P. W. Anderson and J. M. Rowell, "Probable observation of the josephson superconducting tunneling effect," *Phys. Rev. Lett.*, vol. 10, pp. 230–232, Mar 1963. [Online]. Available: https://link.aps.org/doi/10.1103/PhysRevLett.10.230

[14] R. L. Fagaly, "Superconducting quantum interference device instruments and applications," *Review of Scientific Instruments*, vol. 77, no. 10, p. 101101, 2006. [Online]. Available: https://doi.org/10.1063/1.2354545

[15] M. Hämäläinen, R. Hari, R. J. Ilmoniemi, J. Knuutila, and O. V. Lounasmaa, "Magnetoencephalography—theory, instrumentation, and applications to noninvasive studies of the working human brain," *Rev. Mod. Phys.*, vol. 65, pp. 413–497, Apr 1993. [Online]. Available: https://link.aps.org/doi/10.1103/RevModPhys.65.413

[16] L.-S. D, S. N, and M. F, "The role of magnetoencephalography in the early stages of alzheimer's disease." *Frontiers in neuroscience*, vol. 12, Aug 2018. [Online]. Available: https://www.ncbi.nlm.nih.gov/pmc/articles/PMC6104188/

[17] Y. Makhlin, G. Schn, and A. Shnirman, "Josephson-junction qubits with controlled couplings," *Nature*, vol. 398, no. 6725, pp. 305–307, March 1999. [Online]. Available: https://doi.org/10.1038/18613

[18] K. L. Brown, W. J. Munro, and V. M. Kendon, "Using quantum computers for quantum simulation," *Entropy*, vol. 12, no. 11, pp. 2268–2307, 2010. [Online]. Available: https://www.mdpi.com/1099-4300/12/11/2268

[19] S. A. Harris and V. M. Kendon, "Quantum-assisted biomolecular modelling," *Philosophical Transactions of the Royal Society A: Mathematical, Physical and Engineering Sciences*, vol. 368, no. 1924, pp. 3581–3592, 2010. [Online]. Available: https://royalsocietypublishing.org/doi/abs/10.1098/rsta.2010.0087

[20] L. K. Grover, "A fast quantum mechanical algorithm for database search," in *Proceedings of the twenty-eighth annual ACM symposium on Theory of computing*, 1996, pp. 212–219. [Online]. Available: https://dl.acm.org/doi/pdf/10.1145/237814.237866

[21] A. Schilling, M. Cantoni, J. D. Guo, and H. R. Ott, "Superconductivity above 130 K in the HgBaCaCuO system," *Nature*, vol. 363, pp. 56–58, May 1993. [Online]. Available: https://doi.org/10.1038/363056a0

[22] W. of Science, "Results: 10,478 (from Web of Science Core Collection) you searched for: TOPIC: (cuprate) Timespan: All years. Indexes: SCI-EXPANDED, SSCI, A&HCI, ESCI." [Online]. Available: http://www.webofknowledge.com/WOS

——, "Results: 604 (from Web of Science Core Collection) you searched for: TOPIC: (twisted bilayer graphene) Timespan: All years. Indexes: SCI-EXPANDED, SSCI, A&HCI, ESCI." [Online]. Available: http://www.webofknowledge.com/WOS

[23] J. G. Bednorz and K. A. Müller, "Possible high Tc superconductivity in the Ba- La-Cu- O system," *Zeitschrift für Physik B Condensed Matter*, vol. 64, no. 2, pp. 189–193, 1986. [Online]. Available: http://www.w2agz.com/Library/HTSC%20History/(1986)%20Bednorz%20-%20Mueller,%20Z%20Phys%20B%20(CM)%2064,%20189.pdf

[24] F. C. Zhang and T. M. Rice, "Effective hamiltonian for the superconducting Cu oxides," *Phys. Rev. B*, vol. 37, pp. 3759–3761, Mar 1988. [Online]. Available: https://link.aps.org/doi/10.1103/PhysRevB.37.3759

[25] G.-m. Zhao, H. Keller, and K. Conder, "Unconventional isotope effects in the high-temperature cuprate superconductors," *Journal of Physics: Condensed Matter*, vol. 13, no. 29, p. R569, 2001. [Online]. Available: https://iopscience.iop.org/article/10.1088/0953-8984/13/29/202/meta

[26] A. Saleem and S. Hussain, "Review the high temperature superconductor (HTSC) cuprates-properties and applications," *Journal of Surfaces and Interfaces of Materials*, vol. 1, 12 2013. [Online]. Available: https://www.ingentaconnect.com/content/asp/jsim/2013/00000001/00000002/art00001

[27] Y. Cao, V. Fatemi, S. Fang, K. Watanabe, T. Taniguchi, E. Kaxiras, and P. Jarillo-Herrero, "Unconventional superconductivity in magic-angle graphene superlattices," *Nature*, vol. 556, pp. 43–50, Apr 2018. [Online]. Available: https://doi.org/10.1038/nature26160

[28] R. Bistritzer and A. H. MacDonald, "Moiré bands in twisted double-layer graphene," *Proceedings of the National Academy of Sciences*, vol. 108, no. 30, pp. 12 233–12 237, 2011. [Online]. Available: pnas.org/content/108/30/12233.short

[29] J. L. Dos Santos, N. Peres, and A. C. Neto, "Graphene bilayer with a twist: Electronic structure," *Physical review letters*, vol. 99, no. 25, p. 256802, 2007. [Online]. Available: https://journals.aps.org/prl/abstract/10.1103/PhysRevLett.99.256802

[30] C. Lee, X. Wei, J. W. Kysar, and J. Hone, "Measurement of the elastic properties and intrinsic strength of monolayer graphene," *Science*, vol. 321, no. 5887, pp. 385–388, 2008. [Online]. Available: https://science.sciencemag.org/content/321/5887/385

[31] J. S. Bunch, S. S. Verbridge, J. S. Alden, A. M. van der Zande, J. M. Parpia, H. G. Craighead, and P. L. McEuen, "Impermeable atomic membranes from graphene sheets," *Nano Letters*, vol. 8, no. 8, pp. 2458–2462, 2008, pMID: 18630972. [Online]. Available: https://doi.org/10.1021/nl801457b

[32] R. R. Nair, P. Blake, A. N. Grigorenko, K. S. Novoselov, T. J. Booth, T. Stauber, N. M. R. Peres, and A. K. Geim, "Fine structure constant defines visual transparency of graphene," *Science*, vol. 320, no. 5881, pp. 1308–1308, 2008. [Online]. Available: https://science.sciencemag.org/content/320/5881/1308

[33] S. V. Morozov, K. S. Novoselov, M. I. Katsnelson, F. Schedin, D. C. Elias, J. A. Jaszczak, and A. K. Geim, "Giant intrinsic carrier mobilities in graphene and

its bilayer," *Phys. Rev. Lett.*, vol. 100, p. 016602, Jan 2008. [Online]. Available: https://link.aps.org/doi/10.1103/PhysRevLett.100.016602

[34] A. A. Balandin, "Thermal properties of graphene and nanostructured carbon materials," *Nature Materials*, vol. 10, pp. 569–581, Aug 2011. [Online]. Available: https://doi.org/10.1038/nmat3064

[35] S. Manchala, V. Tandava, D. Jampaiah, S. K. Bhargava, and V. Shanker, "Novel and highly efficient strategy for the green synthesis of soluble graphene by aqueous polyphenol extracts of eucalyptus bark and its applications in high-performance supercapacitors," *ACS Sustainable Chemistry & Engineering*, vol. 7, no. 13, pp. 11 612–11 620, 2019. [Online]. Available: https://pubs.acs.org/doi/abs/10.1021/acssuschemeng.9b01506

[36] B. A. Lehner, V. A. Janssen, E. M. Spiesz, D. Benz, S. J. Brouns, A. S. Meyer, and H. S. van der Zant, "Creation of conductive graphene materials by bacterial reduction using shewanella oneidensis," *ChemistryOpen*, vol. 8, no. 7, pp. 888–895, 2019. [Online]. Available: https://chemistry-europe.onlinelibrary.wiley.com/doi/full/10.1002/open.201900186

[37] R. M. Westervelt, "Graphene nanoelectronics," *Science*, vol. 320, no. 5874, pp. 324–325, 2008. [Online]. Available: https://science.sciencemag.org/content/320/5874/324

[38] T. Mahmoudi, Y. Wang, and Y.-B. Hahn, "Graphene and its derivatives for solar cells application," *Nano Energy*, vol. 47, pp. 51 – 65, 2018. [Online]. Available: http://www.sciencedirect.com/science/article/pii/S2211285518301150

[39] S. Song, H. Shen, Y. Wang, X. Chu, J. Xie, N. Zhou, and J. Shen, "Biomedical application of graphene: From drug delivery, tumor therapy, to theranostics," *Colloids and Surfaces B: Biointerfaces*, vol. 185, p. 110596, 2020. [Online]. Available: http://www.sciencedirect.com/science/article/pii/S0927776519307404

[40] D. Akinwande, L. Tao, Q. Yu, X. Lou, P. Peng, and D. Kuzum, "Large-area graphene electrodes: Using CVD to facilitate applications in commercial touchscreens, flexible nanoelectronics, and neural interfaces." *IEEE Nanotechnology Magazine*, vol. 9, no. 3, pp. 6–14, 2015. [Online]. Available: https://ieeexplore.ieee.org/abstract/document/7151823

[41] I. A. Kinloch, J. Suhr, J. Lou, R. J. Young, and P. M. Ajayan, "Composites with carbon nanotubes and graphene: An outlook," *Science*, vol. 362, no. 6414, pp. 547–553, 2018. [Online]. Available: https://science.sciencemag.org/content/362/6414/547

[42] N. D. Mermin, "Crystalline order in two dimensions," *Phys. Rev.*, vol. 176, pp. 250–254, Dec 1968. [Online]. Available: https://link.aps.org/doi/10.1103/PhysRev.176.250

[43] K. S. Novoselov, A. K. Geim, S. V. Morozov, D. Jiang, Y. Zhang, S. V. Dubonos, I. V. Grigorieva, and A. A. Firsov, "Electric field effect in atomically thin carbon films," *Science*, vol. 306, no. 5696, pp. 666–669, 2004. [Online]. Available: https://science.sciencemag.org/content/306/5696/666

[44] J. C. Meyer, A. K. Geim, M. I. Katsnelson, K. S. Novoselov, T. J. Booth, and S. Roth, "The structure of suspended graphene sheets," *Nature*, vol. 446, no. 30, pp. 60–63, Mar 2007. [Online]. Available: https://doi.org/10.1038/nature05545

[45] K. S. Novoselov, D. Jiang, F. Schedin, T. J. Booth, V. V. Khotkevich, S. V. Morozov, and A. K. Geim, "Two-dimensional atomic crystals," *Proceedings of the National Academy of Sciences*, vol. 102, no. 30, pp. 10 451–10 453, 2005. [Online]. Available: https://www.pnas.org/content/102/30/10451

[46] M. S. A. Bhuyan, M. N. Uddin, M. M. Islam, F. A. Bipasha, and S. S. Hossain, "Synthesis of graphene," *International Nano Letters*, vol. 6, pp. 65–83, Jun 2016. [Online]. Available: https://doi.org/10.1007/s40089-015-0176-1

[47] S. Das, M. Kim, J. won Lee, and W. Choi, "Synthesis, properties, and applications of 2-D materials: A comprehensive review," *Critical Reviews in Solid State and Materials Sciences*, vol. 39, no. 4, pp. 231–252, 2014. [Online]. Available: https://doi.org/10.1080/10408436.2013.836075

[48] R. Mas-Balleste, C. Gomez-Navarro, J. Gomez-Herrero, and F. Zamora, "2D materials: to graphene and beyond," *Nanoscale*, vol. 3, no. 1, pp. 20–30, 2011. [Online]. Available: https://pubs.rsc.org/lv/content/articlehtml/2011/nr/c0nr00323a

[49] V. W. Brar, A. R. Koltonow, and J. Huang, "New discoveries and opportunities from two-dimensional materials," *ACS Photonics*, vol. 4, no. 3, pp. 407–411, 2017. [Online]. Available: https://doi.org/10.1021/acsphotonics.7b00194

[50] M. Velick and P. S. Toth, "From two-dimensional materials to their heterostructures: An electrochemist's perspective," *Applied Materials Today*, vol. 8, pp. 68 – 103, 2017, 2D Materials in Electrochemistry. [Online]. Available: http://www.sciencedirect.com/science/article/pii/S235294071730080X

[51] T. Niu and A. Li, "From two-dimensional materials to heterostructures," *Progress in Surface Science*, vol. 90, no. 1, pp. 21–45, 2015. [Online]. Available: https://www.sciencedirect.com/science/article/pii/S0079681614000306

[52] H. Wang, F. Liu, W. Fu, Z. Fang, W. Zhou, and Z. Liu, "Two-dimensional heterostructures: fabrication, characterization, and application," *Nanoscale*, vol. 6, pp. 12 250–12 272, 2014. [Online]. Available: http://dx.doi.org/10.1039/C4NR03435J

[53] H. K. Onnes, "Further experiments with liquid helium. L. the persistence of currents without electro-motive force in supra-conducting circuits," *KNAW, Proceedings*, vol. 17 II, pp. 514–519, 1914. [Online]. Available: https://www.dwc.knaw.nl/toegangen/digital-library-knaw/?pagetype=publDetail&pId=PU00012695

[54] A. M. Forrest, "Meissner and Ochsenfeld revisited," *European Journal of Physics*, vol. 4, no. 2, pp. 117–120, apr 1983. [Online]. Available: https://doi.org/10.1088%2F0143-0807%2F4%2F2%2F011

[55] F. London and H. London, "The electromagnetic equations of the supraconductor," *Proceedings of the Royal Society of London. Series A, Mathematical and Physical Sciences*, vol. 149, no. 866, pp. 71–88, 1935. [Online]. Available: http://www.jstor.org/stable/96265

[56] L. Landau and V. Ginzburg, "K teorii sverkhrovodimosti," *Zh. Eksp. Teor. Fiz*, vol. 20, no. 1064, pp. 546–568, 1950.

V. Ginzburg and L. Landau, *On the Theory of Superconductivity*. Springer, 2009. [Online]. Available: https://link.springer.com/chapter/10.1007/978-3-540-68008-6_4

[57] J. Bardeen, L. N. Cooper, and J. R. Schrieffer, "Theory of superconductivity," *Phys. Rev.*, vol. 108, pp. 1175–1204, Dec 1957. [Online]. Available: https://link.aps.org/doi/10.1103/PhysRev.108.1175

[58] NobelPrize.org, "All nobel prizes in physics." [Online]. Available: https://www.nobelprize.org/prizes/lists/all-nobel-prizes-in-physics

[59] [Online]. Available: https://saylordotorg.github.io/text_general-chemistry-principles-patterns-and-applications-v1.0/s16-07-superconductors.html

[60] de:Benutzer:Schwalbe, February 2005. [Online]. Available: https://en.wikipedia.org/wiki/Meissner_effect#/media/File:EfektMeisnera.svg

[61] R. Flükiger, "Overview of superconductivity and challenges in applications," *Reviews of Accelerator Science and Technology*, vol. 5, pp. 1–23, 2012. [Online]. Available: https://www.researchgate.net/publication/273297345_Overview_of_Superconductivity_and_Challenges_in_Applications

[62] M. Chernodub, "Can nothing be a superconductor and a superfluid?" *Proceedings of Science*, 04 2011. [Online]. Available: https://www.researchgate.net/publication/51888877_Can_nothing_be_a_superconductor_and_a_superfluid

[63] A. Migdal, "Interaction between electrons and lattice vibrations in a normal metal," *Sov. Phys. JETP*, vol. 7, no. 6, pp. 996–1001, 1958. [Online]. Available: http://www.w2agz.com/Library/Classic%20Papers%20in%20Superconductivity/Migdal,%20Strong%20e-p%20Interactions,%20Sov-Phys%20JETP%206,%20996%20(1958).pdf

[64] R. M. Fernandes, "Lecture notes: BCS theory of superconductivity." [Online]. Available: https://portal.ifi.unicamp.br/images/files/graduacao/aulas-on-line/fen-emerg/lecture_notes_BCS.pdf

[65] D. K. Efetov, "Towards inducing superconductivity into graphene," Ph.D. dissertation, Columbia University, 2014. [Online]. Available: https://academiccommons.columbia.edu/doi/10.7916/D8VX0F3T

[66] I. Amidror and R. D. Hersch, "The role of fourier theory and of modulation in the prediction of visible moiré effects," *Journal of Modern Optics*, vol. 56, no. 9, pp.

1103–1118, 2009. [Online]. Available: https://www.tandfonline.com/doi/abs/10.1080/09500340902994140

[67] ——, "Mathematical moiré models and their limitations," *Journal of Modern Optics*, vol. 57, no. 1, pp. 23–36, 2010. [Online]. Available: https://www.tandfonline.com/doi/abs/10.1080/09500340903494629

[68] L. Harmuth, *Dictionary of textiles*. Fairchild publishing company, 1915. [Online]. Available: https://archive.org/details/dictionarytexti01harmgoog/page/n6/mode/2up

[69] [Online]. Available: https://www.etymonline.com/word/moire

[70] [Online]. Available: https://commons.wikimedia.org/wiki/File:Peter_der-Grosse_1838.jpg

[71] [Online]. Available: http://www.artnet.com/artists/alexander-roslin/portraet-af-martin-pierre-foache-Odfb1sQrP_DG8q6rTnozdg2

[72] [Online]. Available: http://www.antiquedress.com/item4173.htm

[73] C. A. Sciammarella, "The moiré methoda review," *Experimental mechanics*, vol. 22, no. 11, pp. 418–433, 1982. [Online]. Available: https://link.springer.com/article/10.1007%2FBF02326823

[74] C. A. Walker, "A historical review of moiré interferometry," *Experimental mechanics*, vol. 34, no. 4, pp. 281–299, 1994. [Online]. Available: https://link.springer.com/article/10.1007%2FBF02325143

[75] P. Ifju and B. Han, "Recent applications of moiré interferometry," *Experimental Mechanics*, vol. 50, no. 8, pp. 1129–1147, 2010. [Online]. Available: https://link.springer.com/article/10.1007%2Fs11340-010-9404-9

[76] J. L. Dos Santos, N. Peres, and A. C. Neto, "Continuum model of the twisted graphene bilayer," *Physical Review B*, vol. 86, no. 15, p. 155449, 2012. [Online]. Available: https://journals.aps.org/prb/abstract/10.1103/PhysRevB.86.155449

[77] A. Macridin and G. Sawatzky, "Phonons, charge and spin in correlated systems," Ph.D. dissertation, 2003, date_submitted:2003 Rights: University of Groningen. [Online]. Available: https://www.rug.nl/research/portal/en/publications/phonons-charge-and-spin-in-correlated-systems(d5eafdc2-d500-4fd2-aab0-d8a0d95ad2f0).html

[78] J. Zaanen, S. Chakravarty, T. Senthil, P. Anderson, P. Lee, J. Schmalian, M. Imada, D. Pines, M. Randeria, C. Varma *et al.*, "Towards a complete theory of high T," *Nature Phys*, vol. 2, pp. 138–143, 2006. [Online]. Available: https://www.nature.com/articles/nphys253

[79] B. Keimer, S. A. Kivelson, M. R. Norman, S. Uchida, and J. Zaanen, "From quantum matter to high-temperature superconductivity in copper oxides," *Nature*, vol. 518, no. 7538, pp. 179–186, 2015. [Online]. Available: https://www.nature.com/articles/nature14165

[80] N. Barišić, M. K. Chan, Y. Li, G. Yu, X. Zhao, M. Dressel, A. Smontara, and M. Greven, "Universal sheet resistance and revised phase diagram of the cuprate high-temperature superconductors," *Proceedings of the National Academy of Sciences*, vol. 110, no. 30, pp. 12 235–12 240, 2013. [Online]. Available: https://www.pnas.org/content/110/30/12235.short

[81] H. Motzkau, "File:cuprates phasedigagram en.svg," 2013. [Online]. Available: https://commons.wikimedia.org/wiki/File:Cuprates_phasedigagram_en.svg

[82] S. H. Simon, *The Oxford Solid State Basics*. Great Clarendon Street, Oxford OX2 6DP, United Kingdom: Oxford University Press, 2017.

[83] E. Merzbacher, *Quantum Mechanics*. Inc., 605 Third Avenue, New York, NY 10 158-0012, United States of America: Hamilton Printing Company, 1998.

[84] I. Swart, "Lecture notes 2017-2018 structure of matter," January 2018.